LASER SATURABLE RESONATORS AND CRITERIA FOR THEIR BISTABLE OPERATION

By

Joseph Winslow Austin

SOLID STATE LASER LABORATORY

Scientific Report No. 8

Electronic Sciences Laboratory
University of Southern California
Los Angeles, California 90007

January, 1972

UNCLASSIFIED
Security Classification

DOCUMENT CONTROL DATA - R & D

(Security classification of title, body of abstract and indexing annotation must be entered when the overall report is classified)

1 ORIGINATING ACTIVITY (Corporate author)

Electronic Sciences Laboratory
University of Southern California
Los Angeles, California 90007

2a. REPORT SECURITY CLASSIFICATION

UNCLASSIFIED

2b. GROUP

3 REPORT TITLE

LASER SATURABLE RESONATORS AND CRITERIA FOR THEIR BISTABLE OPERATION

4. DESCRIPTIVE NOTES (Type of report and inclusive dates)

Scientific Interim

5. AUTHOR(S) (First name, middle initial, last name)

Joseph Winslow Austin

6. REPORT DATE	7a. TOTAL NO OF PAGES	7b. NO. OF REFS
January, 1972	126	38

8a. CONTRACT OR GRANT NO	9a. ORIGINATOR'S REPORT NUMBER(S)
AFOSR-71-2066	
b. PROJECT NO 9751-02	Scientific Report Number 8
c. 6144501F	9b OTHER REPORT NO(S) (Any other numbers that may be assigned this report)
d. 681301	AFOSR - TR - 72 - 139

10 DISTRIBUTION STATEMENT

Approved for public release; distribution unlimited.

11 SUPPLEMENTARY NOTES	12 SPONSORING MILITARY ACTIVITY
TECH OTHER	AFOSR (NPP) 1400 Wilson Boulevard Arlington, Virginia 22209

13 ABSTRACT

Even though saturable absorbers have been used in laser systems as passive switches and modulators since 1964, the operation of these absorbers in conjunction with optical resonators has not been adequately described before. The features of this problem are succinctly contained in the problem of a Fabry-Perot resonator containing a saturable absorber. Such a device is called a saturable resonator. Previous treatments of saturable resonators have neglected the optical resonance effects and have used unsuitable models for the saturable absorbers. Now, a general steady-state solution to the performance of the saturable resonator has been obtained and applied to several experimental configurations. This solution was accomplished by first considering a Fabry-Perot interferometer containing an unsaturable absorber. The transmittance, reflectance and absorptance for this case were determined as a function of the phase difference arising from round trip cavity transits. These quantities are parameterized by the mirror reflectivity and the transmittance of the absorber. Next, the absorber was considered to be saturable and was realistically characterized by the model of Huff and DeShazer with some modifications. Most saturable absorbers exhibit a residual absorption and this residual absorption must be included in any model chosen for a saturable absorber. It was just this neglect of the residual absorption that made most previous treatments of the problem

(continued)

DD FORM 1 NOV 68 1473

DOCUMENT CONTROL DATA - R & D

(Security classification of title, body of abstract and indexing annotation must be entered when the overall report is classified)

in error. The behavior of a saturable absorber was characterized by two parameters which are functions of the transition rates and absorption cross-sections. One of these parameters controls the residual absorptivity and shape of the saturation curve while the other determines the intensity range of saturation. Since the transmittance of the saturable absorber is a complicated transcendental function of the incident intensity, the solution must be done numerically with the aid of a computer. The results of these calculations show the existence of the bistable operation of a saturable resonator under certain conditions. The criteria for bistable operation were obtained and found to be dependent on mirror reflectivity, weak-signal absorber transmittance and the absorber parameter involved with the residual absorption. It was determined that this parameter had to be greater than 8.5 in order to get bistable operation.

A single mode giant pulse ruby laser was used to determine the characteristics of several saturable resonators. A search was also conducted to find saturable absorbers which meet the criteria for bistable operation while at the same time obeying the steady-state assumption. The change of the transmission with incident intensity was measured for the organic dyes cryptocyanine and 1, 1′-Diethyl-2, 2′-Dicarbocyanine Iodide (DDI) dissolved in various organic solvents, as well as a Cd:Se:S glass. For the organic dye it was found that the parameters were highly dependent on the solvent. Those absorbers which met the bistable criteria were the semiconductor glass, and both DDI and cryptocyanine dissolved in either acetone or acetonitrile. Experimental results follow the theory but on-resonance matching difficulties have hindered observation of bistable operation for those saturable absorbers which were found to meet the criteria, however, very noticeable pulse shaping was obtained in many cases. The saturable resonator was also tried as a laser cavity dumping device but here large residual absorption and resonance matching problems limited its usefulness.

LASER SATURABLE RESONATORS AND CRITERIA FOR THEIR BISTABLE OPERATION

by

Joseph Jinslow Austin

A Dissertation Presented to the

FACULTY OF THE GRADUATE SCHOOL

UNIVERSITY OF SOUTHERN CALIFORNIA

In Partial Fulfillment of the

Requirements for the Degree

DOCTOR OF PHILOSOPHY

(Physics)

January 1972

IC

UNIVERSITY OF SOUTHERN CALIFORNIA
THE GRADUATE SCHOOL
UNIVERSITY PARK
LOS ANGELES, CALIFORNIA 90007

This dissertation, written by

Joseph Winslow Austin

under the direction of his Dissertation Committee, and approved by all its members, has been presented to and accepted by The Graduate School, in partial fulfillment of requirements of the degree of

DOCTOR OF PHILOSOPHY

Charles J. Mayo
Dean

Date February 1972

DISSERTATION COMMITTEE

Larry G. Deshazer
Chairman
John Marbarger
William H. Steier

id

ABSTRACT

Even though saturable absorbers have been used in laser systems as passive switches and modulators since 1964, the operation of these absorbers in conjunction with optical resonators has not been adequately described before. The features of this problem are succinctly contained in the problem of a Fabry-Perot resonator containing a saturable absorber. Such a device is called a saturable resonator. Previous treatments of saturable resonators have neglected the optical resonance effects and have used unsuitable models for the saturable absorbers. Now, a general steady-state solution to the performance of the saturable resonator has been obtained and applied to several experimental configurations. This solution was accomplished by first considering a Fabry-Perot interferometer containing an unsaturable absorber. The transmittance, reflectance and absorptance for this case were determined as a function of the phase difference arising from round trip cavity transits. These quantities are parameterized by the mirror reflectivity and the transmittance of the absorber. Next, the absorber was considered to be saturable and was realistically characterized

by the model of Huff and DeShazer with some modifications. Most saturable absorbers exhibit a residual absorption and this residual absorption must be included in any model chosen for a saturable absorber. It was just this neglect of the residual absorption that made most previous treatments of the problem in error. The behavior of a saturable absorber was characterized by two parameters which are functions of the transition rates and absorption cross-sections. One of these parameters controls the residual absorptivity and shape of the saturation curve while the other determines the intensity range of saturation. Since the transmittance of the saturable absorber is a complicated transcendental function of the incident intensity, the solution must be done numerically with the aid of a computer. The results of these calculations show the existence of the bistable operation of a saturable resonator under certain conditions. The criteria for bistable operation were obtained and found to be dependent on mirror reflectivity, weak-signal absorber transmittance and and the absorber parameter involved with the residual absorption. It was determined that this parameter had to be greater than 8.5 in order to get bistable operation.

A single mode giant pulse ruby laser was used to determine the characteristics of several saturable

resonators. A search was also conducted to find saturable absorbers which meet the criteria for bistable operation while at the same time obeying the steady-state assumption. The change of the transmission with incident intensity was measured for the organic dyes cryptocyanine and 1, 1'-Diethyl-2, 2'-Dicarbocyanine Iodide (DDI) dissolved in various organic solvents, as well as a Cd:Se:S glass. For the organic dye it was found that the parameters were highly dependent on the solvent. Those absorbers which met the bistable criteria were the semiconductor glass, and both DDI and cryptocyanine dissolved in either acetone or acetonitrile. Experimental results follow the theory but on-resonance matching difficulties have hindered observation of bistable operation for those saturable absorbers which were found to meet the criteria, however very noticeable pulse shaping was obtained in many cases. The saturable resonator was also tried as a laser cavity dumping device but here large residual absorption and resonance matching problems limited its usefulness.

ACKNOWLEDGEMENTS

The author's sincere thanks go to Professor Larry DeShazer for his continual encouragement and invaluable advice and support during the course of this study.

For suggestions and assistance relating specifically to this thesis the author wishes to thank Professor Abraham Szöke and Professor Joel Parks.

The technical assistance of E.A. Maunders, H.R. Owen, Jr., and J.C. Emerson is very much appreciated. Marjorie Judge was especially helpful with the typing.

The author's deepest appreciation is reserved for his wife and his parents. Without their patience, understanding, and unbounded support this work would not have been possible.

TABLE OF CONTENTS

	Page
ABSTRACT	ii
ACKNOWLEDGEMENTS	v
LIST OF ILLUSTRATIONS	ix
CHAPTER	
I. INTRODUCTION	1
A. Motivation for This Study	1
B. History	2
II. GENERAL THEORY OF SATURABLE ABSORBER	6
A. Fabry-Perot Interferometer Containing Unsaturable Absorber	6
1. Introduction	6
2. Corrected Mirror Loss Derivation	9
3. Derivation of Transmission, Reflection and Absorption of the Fabry-Perot Interferometer with Internal Loss	13
4. Resonance Behavior	20
5. Effects of Absorption	25
6. Szöke Approximation	27
B. Characteristics of Saturable Absorbers	32
1. Description of Saturable Absorbers	32
2. Review of Excited State Absorption Model	34

CHAPTER Page

3. Energy Level Scheme for Organic Dyes 35

4. Excited State Absorption Model Saturation Equation 38

5. Residual Absorption Model 41

6. Justification of Excited State Absorption Model 42

7. Solvent Effects 47

8. Semiconductor Glass Saturable Absorbers 50

9. Single Absorption with Unsaturable Loss 52

10. General Parametrization of Saturable Absorbers 56

C. Fabry-Perot Interferometer with a Saturable Absorber 60

1. Coupling of Fabry-Perot Interferometer with Saturable Absorber 60

2. Properties 64

3. Criteria for Bistable Operation 68

4. Pulse Shaping 71

III. THE EXPERIMENT 79

A. The Laser 79

B. Search for Proper Saturable Absorber 83

1. Experimental Set-up 83

2. Results 87

a. 1,1'-diethyl-2,2'-dicarbocyanine iodide in methanol 87

CHAPTER Page

b. 1,1'-diethyl-2,2'-dicarbocyanine iodide in acetonitrile 89

c. 1,1'-diethyl-2,2'-dicarbocyanine iodide in acetone 89

d. Cryptocyanine in acetonitrile 89

e. Cryptocyanine in acetone 93

f. Semiconductor Glass Saturable Absorber 93

C. The Saturable Resonator Using Cryptocyanine in Methanol 96

1. Experimental Set-up 96

2. Results 100

D. Saturable Resonator with Absorber Meeting Bistable Criteria 106

1. Experimental Set-up 106

2. Results 107

a. Organic Dyes 107

b. Semiconductor Glass Saturable Absorber 109

IV. CONCLUSIONS 111

A. Theory 111

B. Experimental Verification 113

C. Further Work 116

APPENDIX A. LASER ALIGNMENT 118

APPENDIX B. ERROR ARISING FROM MEASUREMENT OF GAUSSIAN BEAM WITH A FINITE SIZED PINHOLE ... 120

APPENDIX C. FURTHER DESCRIPTION OF OPTICAL ISOLATOR. 122

REFERENCES 124

LIST OF ILLUSTRATIONS

Figure		Page
II.A.1.	Ray diagram for mirror loss derivation	11
II.A.2.	Ray diagram for intracavity loss derivation.	14
II.A.3.	Resonance behavior of the interferometer ...	21
II.A.4.	Variation of F with T_α	24
II.A.5.	Variation of maximum transmittance, maximum absorptance, and minimum reflectance of an interferometer with T_α	26
II.A.6.	Comparison of Szöke's approximation to the exact solution for transmission versus loss.	31
II.B.1.	Excited triplet state absorption energy level model from Huff and DeShazer	37
II.B.2.	Energy level diagram for both excited singlet state and excited triplet state absorption..	43
II.B.3.	Band structure in k-space for semiconductor saturable absorber	51
II.B.4.	Energy level diagram for single absorption with unsaturable loss	53
II.B.5.	Plot of the saturation equation for several values of D_1.....	57
II.B.6.	Plot of the saturation equation for various values of D_2.....	59
II.C.1.	The standing wave in the cavity results from the two traveling waves I_+ and I_-	61
II.C.2.	Input versus output of the saturable resonator for different values of R, T_0 and D_1.....	65
II.C.3.	Illustration of bistable operation and the optical hysteresis loop	67

Figure		Page
II.C.4.	Bistable criteria for T_0 vs $1/D_1$ and various R. The region above each curve corresponds to bistable region	72
II.C.5.	Bistable criteria for R vs $1/D_1$ and various T_0	73
II.C.6.	Pulse shaping for a saturable resonator operating in the bistable region	74
II.C.7.	Resultant pulses arising from different relative values of I_0 and I_p	76
II.C.8.	Pulse shaping for a saturable resonator operating in the normal region	77
III.A.1.	The ruby laser	80
III.B.1.	Experimental configuration	85
III.B.2.	DDI dissolved in methanol	88
III.B.3.	DDI dissolved in acetonitrile	90
III.B.4.	DDI dissolved in acetone	91
III.B.5.	Cryptocyanine dissolved in acetonitrile	92
III.B.6.	Cryptocyanine dissolved in acetone	94
III.B.7.	Semiconductor saturable absorber	95
III.C.1.	Saturable resonator construction for experiment with organic dye solutions	97
III.C.2.	Experimental configuration for saturable resonator	99
III.C.3.	Experimental data points and theoretical curve for saturable resonator containing cryptocyanine in methanol	102
III.C.4.	Experimental data points and theoretical curve for saturable resonator containing cryptocyanine in methanol	103

Figure Page

III.C.5. Pulse narrowing from the saturable resonator 104

III.C.6. Effects of several components of the saturable resonator..... 105

I. INTRODUCTION

A. Motivation for this Study.

The saturable resonator was recently proposed[1,2] for use as a passive light switch. With the combination of a saturable absorber and a Fabry-Perot interferometer cavity it is possible to obtain much more pronounced "on" and "off" conditions than with the saturable absorber separately. For this reason alone it would be of interest to study the saturable resonator.

A more important reason however, for studying the saturable resonator is that the combination of a Fabry-Perot interferometer and a saturable absorber is an integral part of many Q-switched laser systems. The understanding of the saturable resonator will then help in the development of Q-switched lasers.

Much of the work to date has dealt with inadequate models for saturable absorbers. In the work presented here, the consequences of this inadequacy will be compared with the results of more realistic absorber models. It will be shown that a limiting factor in the operation of the saturable resonator is the residual absorption present in most saturable absorber systems.

Methods of reducing this residual absorption in organic dye saturable absorber systems will be discussed. This should also prove useful in the operation of Q-switched laser systems using organic dye saturable absorbers. It will also be shown that significant pulse shaping can be obtained by properly adjusting the saturable resonator parameters.

B. History.

Saturable absorbers, that is absorbers whose transmittance depends on the intensity of the incident light, have proven to be very important for use in laser systems. They are primarily used as passive light switches[3-8] and modulators[9-11] in laser cavities. Much of the previous work has involved a search for proper materials. More recently, however, interest has shifted to the mechanisms of this saturation.[12-15] This interest has been primarily in organic compounds since these compounds are more resistant to damage.

Hercher et al.[13,16] did much work on phthalocyanine and phthalocyanine metal dyes and showed that relaxation times prohibit using the steady state approximation for light pulses in the 10 nsec. range. These workers used both an excited singlet state absorption model and an excited triplet state absorption model to

explain the residual absorption. They concluded that the excited singlet state absorption was the important factor for residual absorption in phthalocyanine dyes. Huff and DeShazer[12,17,18] were able to characterize several dye systems, in both steady state and nonsteady state, using an excited triplet state absorption model for the residual absorption. Using a steady state model with excited triplet state absorption an excellent fit of the saturation of cryptocyanine in methanol was obtained.

There are other systems particularly semiconductor saturable absorbers[6] and gas systems such as SF_6[19,20] which have been studied. Development of dye laser systems too, has prompted much interest in the absorption of light by organic compounds. It has been shown that quenching the triplet state[21] in these dye compounds greatly enhances the operation of these dye lasers.

The characteristics of a classical Fabry-Perot interferometer are presented in most texts on optics, e.g., Born and Wolf.[22] In most applications of a Fabry-Perot interferometer it is desirable to have as little loss as possible inside the cavity so most treatments of the Fabry-Perot interferometer are done in the regime of low loss. The classical treatments [22,23] usually add the cavity loss to the solution of the lossless cavity giving only a partially correct answer.

Bjorkholm[1] proposed using a Fabry-Perot interferometer containing a saturable absorber as an output coupling element of a Q-switched laser. He wanted a way of more efficiently coupling the energy out of a Q-switched laser after the pulse was formed. The peak output powers of the laser would be improved if the transmission of the output reflector was increased just before the pulse reached its maximum intensity. The energy contained in the cavity could then theoretically be removed from the cavity in one round trip transit if the transmission became unity.

Independently Szöke, et al.[2] proposed the saturable absorber as a bistable optical element. Using a two level model for the saturable absorber these workers demonstrated that bistable operation was theoretically possible under certain conditions. The two level model, however, did not include residual absorption and therefore limited its usefulness for many saturable absorber systems. Szöke obtained shorter pulses (on the order of a cavity transit time) out of a Q-switched CO_2 laser system using a saturable resonator containing SF_6 as the output element. The saturable resonator was not used as a separate element in this work.

Szöke, et al.[2] proposed several other uses for the saturable resonator. Since the saturable resonator

has a bistable property it could be used as an optical memory element. When operating out of the bistable region the variable reflectivity can act as a laser stabilizer provided the time behavior of the system does not become unstable.

When operating off resonance the reflectivity increases with increasing intensity so in this mode it can act as a Q-switching element. Coupling the saturable resonator with another interferometer cavity gives a monostable multivibrator. With this it would be possible to produce a train of pulse from a cw light source provided the saturable resonator is operated in the bistable region.

Spiller[24] has done some work with the saturable resonator simultaneous to the work presented here. He uses an optically thin approximation for the mirror separation and also uses a two level model for the saturable absorber. He includes a linear (or non-saturable) loss term attributed to the cavity loss or the absorber residual absorption. In his work this linear loss is an adjustable parameter of the system. Spiller has observed pulse shortening of a ruby laser pulse using phthalocyanine dyes in the saturable resonator. No criteria was established for the bistable operation of the saturable resonator in this work.

II. GENERAL THEORY OF SATURABLE RESONATOR

A. Fabry-Perot Interferometer Containing Unsaturable Absorber.

1. Introduction

A study of a Fabry-Perot interferometer containing an absorber which is not saturable is the first step to the solution of the saturable resonator problem. Subsequently, the solution of the Fabry-Perot interferometer with unsaturable absorption will be extended by allowing the absorptivity to be a function of the incident intensity. If a model of the saturable absorber is specified this nonlinear absorption behavior can be coupled with the interferometer results to give a solution for the saturable resonator.

The well-known classical solution to the Fabry-Perot interferometer involves the superposition of an incoming wave of wavelength λ, with its resulting multiple reflections and transmissions.[22,23] The resulting multiple-beam interference is obtained by summing over the individual components taking into account the phase changes upon reflection and phase differences arising from cavity transits. The equations for the transmitted (I_T) and reflected (I_R) intensities for an incident

intensity (I_i) are given by the following equations

$$\frac{I_T}{I_i} = \frac{T^2}{(1-R)^2 + 4R \sin^2 \delta/2} \tag{1}$$

and

$$\frac{I_R}{I_i} = \frac{4R \sin^2 \delta/2}{(1-R)^2 + 4R \sin^2 \delta/2} \tag{2}$$

where δ is the cavity round trip phase difference, T and R are the transmittance and reflectance of either mirror of the interferometer. For lossless mirrors

$$T + R = 1 \tag{3}$$

Letting $F = \frac{4R}{(1-R)^2}$

these equations become

$$\frac{I_T}{I_i} = \frac{1}{1 + F \sin^2 \delta/2} \tag{4}$$

and

$$\frac{I_R}{I_i} = \frac{F \sin^2 \delta/2}{1 + F \sin^2 \delta/2} \tag{5}$$

This type of solution is given in many texts, e.g., Born and Wolf.[22] However, no previous treatment includes an absorption inside the interferometer cavity. Some treatments do include absorption by the mirrors, e.g. Tolansky,[23] or Born and Wolf,[22] but these results are quite different than for intracavity absorption. The most common method of including mirror loss is to assume that the mirror parameters obey the following relation

$$R + T + A = 1 \tag{6}$$

where again R is the reflectance, T the transmittance, and A the absorptance of a mirror.[22] Equation (4) for the transmitted intensity now becomes

$$\frac{I_T}{I_i} = \left(1 - \frac{A}{1 - R}\right)^2 \frac{1}{1 + F \sin^2 \delta/2} \tag{7}$$

In deriving equation (2) for the interferometer reflectance the assumption was made that R + T = 1 for each mirror, so most treatments ignore rederiving the reflectance of the Fabry-Perot interferometer for the loss case. Tolansky[22] attempts to do this derivation by assuming that R is the same in both equations (3) and (6) but the total transmission (T') of a mirror changes due to the loss in the

mirror. T and T' are then related by some constant, that is

$$\frac{T'}{T} = K \tag{8}$$

where $K \leq 1$.

Figure II.A.1 shows a ray diagram of how the reflections must occur in Tolansky's derivation. Tolansky, however, considers the on-resonance case and tries to deal only with intensities.

2. Corrected Mirror Loss Derivation

To obtain the reflected intensities from Figure II.A.1 it is first necessary to sum the reflected amplitudes. This gives

$$A_r = -\rho A_i + \rho t'^2 e^{i\delta} A_i + \rho^3 t'^2 e^{2i\delta} A_i + \ldots$$

where A_i is the incident intensity, A_r the reflected intensity, ρ the amplitude reflection coefficient, t' the amplitude transmission coefficient and δ the phase difference from a round trip cavity transit. The above equation can be summed to give

$$\frac{A_r}{A_i} = -\rho\left[1 - \frac{t'^2 e^{i\delta}}{1 - \rho^2 e^{i\delta}}\right]$$

$$= -\rho\left[\frac{1 - (\rho^2 + t'^2)e^{i\delta}}{1 - \rho^2 e^{i\delta}}\right] \qquad (9)$$

Taking the absolute value and squaring both sides gives the following intensity relationship

$$\frac{I_R}{I_i} = R\left[\frac{1 + (R + T')^2 - 2(R + T')\cos\delta}{1 + R^2 - 2R\cos\delta}\right]$$

But T' is also given by

$$T' = T(1-A)$$

giving

$$\frac{I_R}{I_i} = R\left[\frac{A^2(1 + T)^2 + 4(1 - A(1+T))\sin^2\delta/2}{(1 - R)^2 + 4R\sin^2\delta/2}\right] \qquad (1$$

Similarly summing the transmitted amplitudes gives

$$A_t = t'A_i + \rho^2 t'^2 e^{i\delta} A_i + \rho^4 t'^2 e^{2i\delta} A_i + \ldots$$

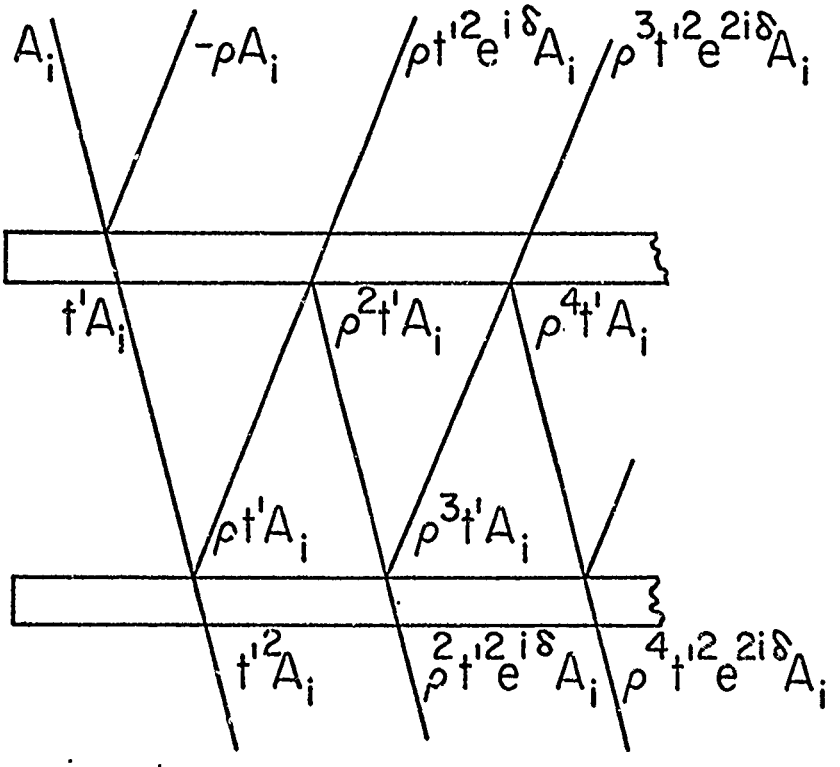

Figure II.A.1. Ray diagram for mirror loss derivation.

thus

$$\frac{A_t}{A_i} = \frac{t'^2}{1 - \rho^2 e^{i\delta}} \quad . \tag{11}$$

This yields the following intensity relationship

$$\frac{I_T}{I_i} = \frac{T'^2}{1 + R^2 - 2R\cos\delta}$$

$$= \frac{T'^2}{(1 - R)^2} \left[\frac{1}{1 + F \sin^2\delta/2}\right]$$

$$= \frac{T^2(1 - A)^2}{(1 - R)^2} \quad \frac{1}{1 + F \sin^2\delta/2}$$

so

$$\frac{I_T}{I_i} = (1 - \frac{A}{1 - R})^2 (1 - A)^2 \quad \frac{1}{1 + F \sin^2\delta/2} \tag{12}$$

where

$$F = \frac{4R}{(1 - R)^2} \quad . \tag{13}$$

Except for the factor of $(1 - A)^2$ this is identical to equation (7).

The above arguments are a good approximation for thin metal film reflectors since the reflection arises in large part from the first surface reflection. However, for thin film dielectric reflectors the absorption, A, will greatly affect the reflection R, of the film. This is because thin dielectric film reflectors work on the same principle as the Fabry-Perot interferometer and loss in the film appears as an intracavity loss. This is the subject of the next section.

3. Derivation of Transmission, Reflection and Absorption of the Fabry-Perot Interferometer with Internal Loss.

Figure II.A.2 shows the multiply reflected, transmitted, and absorbed amplitudes which result from an incident amplitude A_i. For simplicity of illustration the angle of incidence is away from normal but normal incidence is the only case of interest in the saturable resonator.

The reflected amplitude is obtained by summing over all the amplitudes traveling in the backward direction, making sure phase differences are accounted for. This phase difference is due to the path differences of round trip cavity transits. There is another phase change due to reflec-

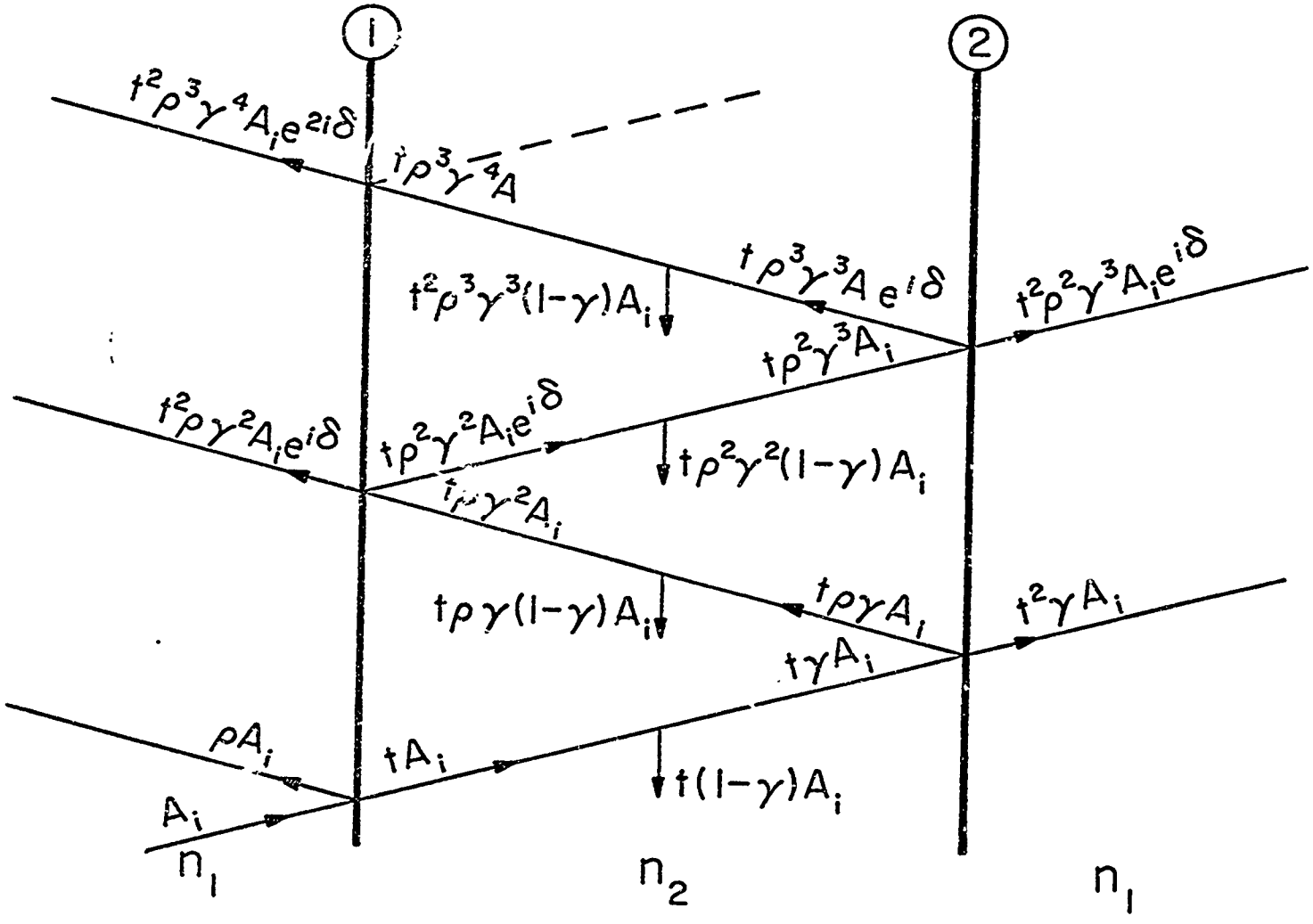

Figure II.A.2. Ray diagram for intracavity loss derivation.

tion at the interface between two materials of different indices. This phase change gives the negative sign to the first reflected beam relative to all other reflections since it is the only one that involves an $n_1 \rightarrow n_2$ interface reflection and must be 180° out of phase with the $n_2 \leftarrow n_1$ interface reflections for normal incidence. Summing the reflected amplitude gives

$$A_r = -\rho A_i + t^2\rho\gamma^2 A_i e^{i\delta} + t^2\rho^3\gamma^4 A_i e^{2i\delta} + \ldots \quad (1)$$

where A_r is the reflected amplitude, A_i is the incident amplitude, ρ and t are the amplitude reflection and transmission coefficients respectively, $\gamma = e^{-(\alpha/2)L}$, where α is the intensity absorption coefficient of the material in the cavity, $\delta = \frac{4\pi L n_2}{\lambda}$, L the mirror separation ($L > \lambda$), and n_1 and n_2 are the indices of refraction of the appropriate media. From this the following ratio is obtained

$$\frac{A_r}{A_i} = -\rho + t^2\gamma^2\rho e^{i\delta} \sum_{m=0}^{\infty} \gamma^{2m}\rho^{2m} e^{im\delta}$$

which can be simplified to

$$\frac{A_r}{A_i} = -\rho \left[1 - \frac{t^2\gamma^2 e^{i\delta}}{1 - \gamma^2\rho^2 e^{i\delta}} \right]$$

$$= -\rho\left[\frac{1 - e^{i\delta}\gamma^2(t^2 + \rho^2)}{1 - \gamma^2\rho^2 e^{i\delta}}\right]$$

However, $t^2 + \rho^2 = 1$ provided there are no losses in the mirrors. This allows further simplification, i.e.,

$$\frac{A_r}{A_i} = -\rho\left[\frac{1 - \gamma^2 e^{i\delta}}{1 - \gamma^2\rho^2 e^{i\delta}}\right] \tag{2}$$

A similar addition of the transmitted amplitudes gives the following equality

$$A_T = t^2\gamma A_i \sum_{m=0}^{\infty} \gamma^{2m}\rho^{2m} e^{im\delta} ,$$

$$\frac{A_T}{A_i} = \frac{t^2\gamma}{1 - \gamma^2\rho^2 e^{i\delta}} \tag{3}$$

Two other quantities of use in finding the intensity absorbed are A_+, the amplitude at mirror 1 traveling toward mirror 2, and A_-, the amplitude at mirror 2 traveling toward mirror 1. These are given by the following

$$A_+ = tA_i \sum_{m=0}^{\infty} \rho^{2m}\gamma^{2m} e^{im\delta}$$

and

$$A_- = t\rho\gamma A_i \sum_{m=0}^{\infty} \rho^{2m}\gamma^{2m}e^{im\delta} \quad .$$

Thus

$$\frac{A_+}{A_i} = \frac{t}{1 - \rho^2\gamma^2 e^{i\delta}} \tag{4}$$

and

$$\frac{A_-}{A_i} = \frac{t\rho\gamma}{1 - \rho^2\gamma^2 e^{i\delta}} \quad . \tag{5}$$

Now $I = |A|^2$ where I is the intensity, so

$$\frac{I_R}{I_i} = R\left[\frac{1 + \gamma^4 - \gamma^2(e^{i\delta} + e^{-i\delta})}{1 + \gamma^4R^2 - \gamma^2R(e^{i\delta} + e^{-i\delta})}\right]$$

$$= R\left[\frac{1 + \gamma^4 - \gamma^2\cos\delta}{1 + \gamma^4R^2 - \gamma^2R\cos\delta}\right] \quad .$$

Letting $\gamma^2 = T_\alpha = e^{-\alpha L}$
and remembering $\cos\delta = 1 - 2\sin^2\delta/2$, then

$$\frac{I_R}{I_i} = \frac{H + F \sin^2 \delta/2}{1 + F \sin^2 \delta/2} \quad . \tag{6}$$

Similarly,

$$\frac{I_T}{I_i} = \frac{(1 - R)^2 T_\alpha}{1 + T_\alpha^2 R^2 - 2T_\alpha R \cos \delta}$$

$$= \frac{G}{1 + F \sin^2 \delta/2} \quad . \tag{7}$$

It is convenient to define the three terms F, G, and H such that

$$F \equiv \frac{4RT_\alpha}{(1 - T_\alpha R)^2} \quad , \tag{8}$$

$$G \equiv \frac{(1-R)^2 T_\alpha}{(1 - T_\alpha R)^2} \tag{9}$$

and

$$H \equiv \frac{R(1 - T_\alpha)^2}{(1 - RT_\alpha)^2} \quad . \tag{10}$$

By similar manipulations

$$\frac{I_+}{I_i} = \frac{G}{T_\alpha(1 - R)(1 + F \sin^2 \delta/2} \tag{12}$$

and

$$\frac{I_-}{I_i} = \frac{GRT_\alpha}{T_\alpha(1 - R)(1 + F \sin^2 \delta/2} \tag{12}$$

The absorbed intensity can be obtained using the following relation

$$I_A = (I_+ + I_-)(1 - T_\alpha)$$

Thus

$$\frac{I_A}{I_i} = \frac{G(1 + RT_\alpha)(1 - T_\alpha)}{T_\alpha(1 - R)(1 + F \sin^2 \delta/2)}$$

$$= \frac{1 - G - H}{1 + F \sin^2 \delta/2} \tag{13}$$

In retrospect it is seen that this result could be obtained from

$$\frac{I_A}{I_i} = 1 - \frac{I_R}{I_i} - \frac{I_T}{I_i}$$

as expected. It is interesting to note that the absorbed intensity has the same resonance behavior as do the transmitted and reflected intensities. This arises because the intensity inside the cavity of course shows a resonance behavior. Since the absorption is proportional to the intracavity intensity it too shows a resonance.

4. Resonance Behavior

The terms I_N/I_i (N = T,R or A) give the resonance behavior of the system with variation of δ. The resonance behavior for several values of T_α is shown in Figure II.A.3. It should be noticed for $\delta = 2m\pi$ where m = integer, that

$$\frac{I_R}{I_i} = H$$

$$\frac{I_T}{I_i} = G$$

and

$$\frac{I_A}{I_i} = 1 - G - H.$$

Thus H is the minimum reflectance and G is the maximum transmittance of the interferometer. It should also be noticed that the width of the resonances change greatly

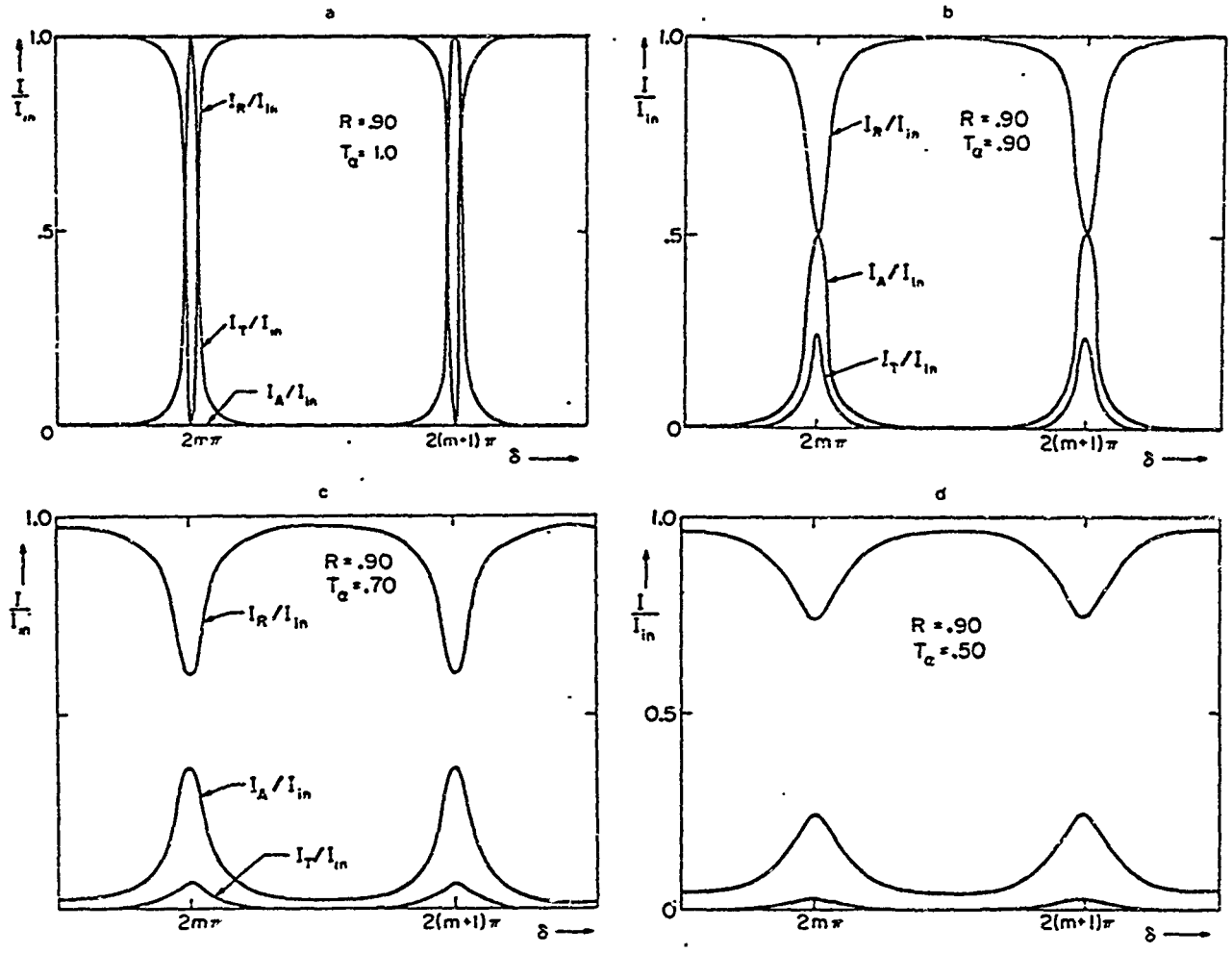

Figure II.A.3. Resonance behavior of the interferometer for (a) $T_\alpha = 1.0$, (b) $T_\alpha = 0.9$, (c) $T_\alpha = 0.7$, and (d) $T_\alpha = 0.5$.

with variation in T_α. F is related to the full width at half-maximum of the resonance and can be found by determining the value of δ at which the transmittance goes to one-half the peak value,[22] i.e.,

$$\frac{I_T}{I_i}(\delta) = \frac{1}{2}\left[\frac{I_T}{I_i}\right]_{max}.$$

From equation (7) it is easy to see that this occurs for $\delta = \delta_{1/2}$ where $\delta_{1/2} = 2m\pi + x$ and $2x$ is the full width at half maximum. $\delta_{1/2}$ can be obtained from

$$\sin^2 \delta_{1/2} = \sin^2 (m\pi \pm x/2) = F.$$

Thus $|x|/2 = \sin^{-1} 1/\sqrt{F}$ gives the points of half maximum. For there to be a half maximum in the transmission function, however, F must be greater than unity. If this is not true then sin $|x|/2$ would be greater than unity which is of course not possible. This means that the transmission of the interferometer does not go one half the peak value for F less than unity. The restriction on F then yields

$$F = \frac{4RT_\alpha}{(1 - RT_\alpha)^2} \geq 1$$

and solving this equality for RT_α gives

$$RT_\alpha \geq 3 - 1/2\sqrt{32} \approx .17.$$

With this restriction on RT_α, the half width is then

$$FWHM = 2x = 4 \sin^{-1} 1/\sqrt{F}$$

and for large F

$$\sin^{-1} 1/\sqrt{F} \approx 1/\sqrt{F}$$

giving $FWHM = 4/\sqrt{F}$.

This is related to the classical finesse[22], Φ, by

$$\Phi = \frac{2\pi}{2x}$$

$$= \frac{\pi}{2 \sin^{-1} 1/\sqrt{F}}$$

$$\Phi \approx \frac{\pi\sqrt{F}}{2} \qquad \text{(for large F only).}$$

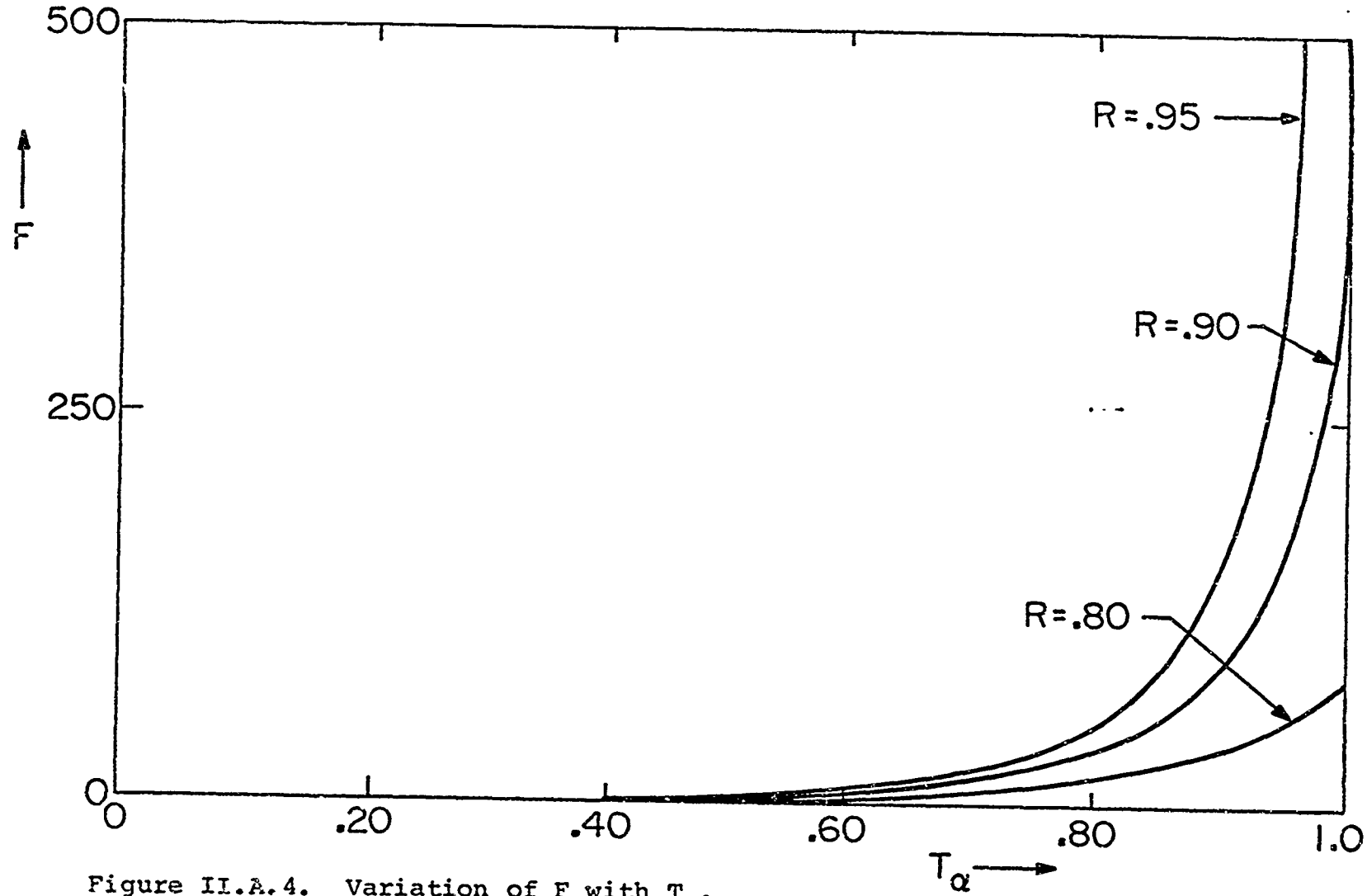

Figure II.A.4. Variation of F with T_α.

5. Effects of Absorption

It is seen from equation (8), Section II.B.3 that as $T_\alpha \to 0$, $F \to 0$ and the resonance peaks become very broad. At the other limit, $T_\alpha \to 1$, and $F = 4R/(1-R)^2$, which is the usual result for no absorber between the mirrors. Figure II.A.4 shows the variation of F with T_α for several different mirror reflectivities. Figure II.A.5 shows the functional dependence of the maximum transmittance G, the minimum reflectance H, and the maximum absorptance A (A = 1 - G - H) on the absorber transmissivity T_α. This is shown for several values of mirror reflectance. It should be noted that as $T_\alpha \to 0$, $H \to R$, $G \to 0$ and $A \to 1-R$. In other words, the system looks like a mirror with reflectivity R where everything transmitted through the first mirror is absorbed. As T_α increases, the maximum transmission increases monotonically to unity and the minimum reflection decreases monotonically to zero. It is also seen in Figure II.A.5 that for certain values of mirror reflectivity the absorption, A, has an extremal value for variation of T_α. This extreme can be found by using equations 9 and 10 to give A in terms of T_α. This gives

$$A = 1 - G - H$$

$$= 1 - \frac{(1-R)^2 T_\alpha + R(1-T_\alpha)^2}{(1 - RT_\alpha)^2} \qquad (1)$$

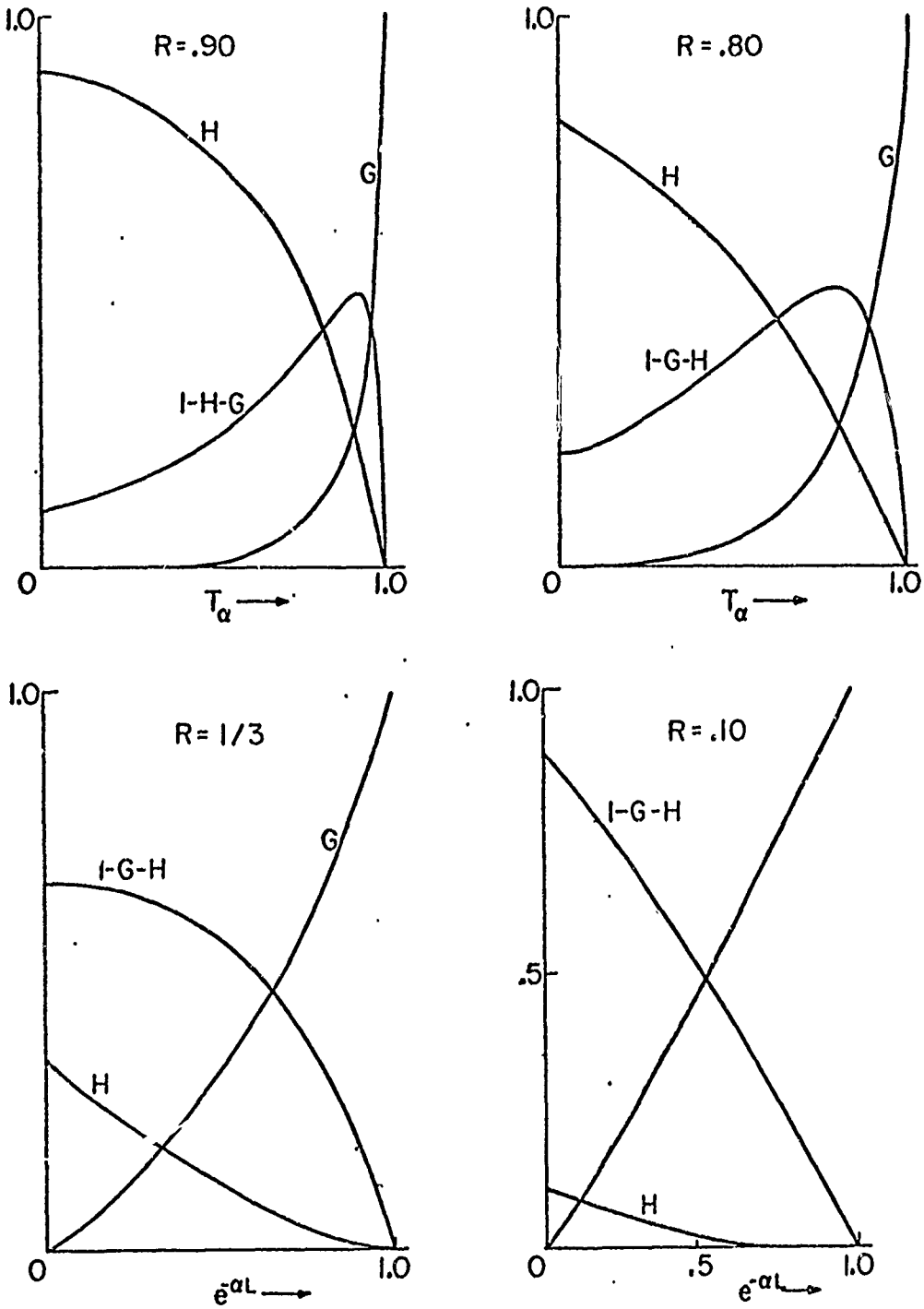

Figure II.A.5. Variation of maximum transmittance, maximum absorptance, and minimum reflectance of an interferometer with T_α.

Taking the derivative

$$\frac{d\Lambda}{dT_\alpha} = -\left[\frac{(1-RT_\alpha)^2((1-R)^2 - 2R(1-T_\alpha))}{(1-RT_\alpha)^4} \right.$$

$$\left. - \frac{[(1-R)^2 T_\alpha + R(1-T_\alpha)^2](-2R)(1-RT_\alpha)}{(1-RT_\alpha)^4} \right]$$

Setting the derivative equal to zero and solving for $(T_\alpha)_{max}$ gives

$$(T_\alpha)_{max} = \frac{3R-1}{R(3-R)} . \qquad (2)$$

This gives

$$A_{max} = \frac{(R+1)^2}{8R} \qquad (3)$$

Now since $0 \leq T \leq 1$, equation 14 implies that the minimum value of R which will give a maximum to A is $R = 1/3$.

6. Szöke Approximation[2]

To compare the exact results to the approximate solution used by Szöke for R~1, first consider G which is the on resonance or maximum transmission,

$$G = \frac{(1-R)^2 T_\alpha}{(1-RT_\alpha)^2} \quad .$$

Szöke takes the limit where T_α is close to unity, then

$$T_\alpha = e^{-\alpha L} \approx 1 - \alpha L. \tag{1}$$

So $$G \approx \frac{(1-R)^2(1-\alpha L)}{(1 - R + R\alpha L)^2}$$

$$= \frac{1 - \alpha L}{\left(1 + \frac{R\alpha L}{1-R}\right)^2}$$

and if $\alpha L \ll L$

$$G \approx \frac{1}{(1 + k)^2} \tag{2}$$

where $k = R\alpha L/(1-R)$ is Szöke's "strength of resonance". Similarly, for the minimum reflection, H

$$H = \frac{R(1-T_\alpha)^2}{(1 - RT_\alpha)^2}$$

$$\approx \frac{R(1 - 1 + \alpha L)^2}{(1 - R + R\alpha L)^2}$$

$$= \frac{\frac{(R\alpha L)^2}{(1 - R)^2}}{R\left(1 + \frac{R\alpha L}{1 - R}\right)^2}$$

$$= \frac{k^2}{R(1 + k)^2} \quad . \tag{3}$$

For the maximum absorption

$$1 - G - H = 1 - \frac{R + k^2}{R(1 + k)^2}$$

$$= \frac{R + 2Rk + Rk^2 - R - k^2}{R(1 + k)^2}$$

$$= \frac{k}{(1 + k)^2}\left(2 - \frac{k(1-R)}{R}\right) \quad .$$

But $\quad k\frac{(1-R)}{R} = \alpha L << 1 \quad ,$

So $\quad 1 - G - H = \frac{k}{(1+k)^2}(2 - \alpha L)$

$$\approx \frac{2k}{(1 + k)^2} \quad . \tag{4}$$

The dashed line in Figure II.A.6 shows Szöke's approximation for the maximum transmission.

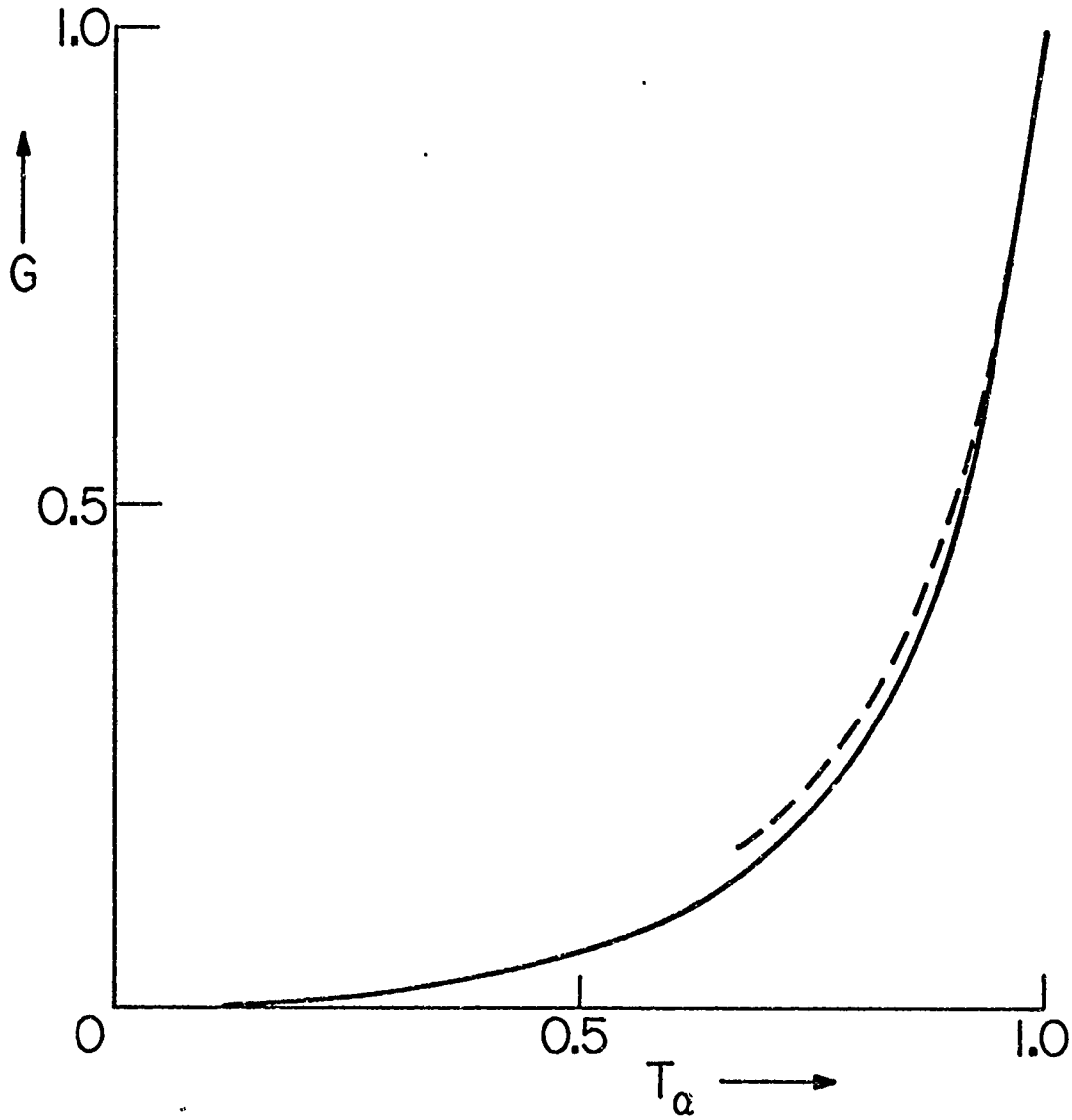

Figure II.A.6. Comparison of Szöke's approximation to the exact solution for transmission versus loss.

B. Characteristics of Saturable Absorbers.

1. Description of Saturable Absorbers

With the Fabry-Perot interferometer problem solved for the case with an unsaturable absorber it is now possible to deal with the case with saturable absorption but first it is necessary to have a model for saturable absorbers. Since a well defined single mode giant pulse ruby laser was available for the experimental work the following discussions will be limited to saturable absorbers used at the ruby wavelength. However, there is no reason to believe that the following discussion does not hold for saturable absorbers used in other laser systems.[13,15] To present the saturable absorbers used with ruby have been principally organic dye compounds but there are some solid state semiconductor type materials which have been developed.[6]

A saturable absorber is basically a material whose transmittance has a functional dependence on the power density incident. Naturally if the fields are intense enough any material will show a saturation of the transmission. For a material to be useful in laser systems it must, of course, show this transmittance saturation in the intensity region in which the laser operates. Usually this transmittance increases with increasing power

density. This increase in transmittance is not to be confused with the phenomena of self-induced transparency. Saturable absorption is not a coherent effect and relies on extraction of energy from the incident beam in order to increase the transmission. For the organic dyes this variation in transmission is due to the saturation of the optical transitions involved in the absorption. For the semiconductor glasses the transmission change is due to shifting of the absorption edge to shorter wavelengths as the power density increases.[6]

For most saturable absorbers there is a residual absorption. The transmission increases rapidly with increasing intensity until it flattens out and approaches a transmittance less than unity. Several phenomenological models have been proposed to deal with this residual absorption, one being an energy level model with excited state absorption developed by Huff and DeShazer.[12] Another model with single absorption and an unsaturable loss will be developed here. The excited state absorption model will be reviewed and compared to the results of the single absorption with an unsaturable loss model. The excited state absorption model is a physically appealing model for organic dye saturable absorbers due to the abundance of states. The linear loss model, on the other hand, is probably more fitting for semiconductor type saturable

absorbers since absorption by conduction band electrons involves indirect transitions ($\Delta\vec{k} \neq 0$) and these transitions are highly improbable. Other characteristics such as intensity levels at which saturation occurs and time response of the system must be described by any chosen model for it to be useful.

2. Review of Excited State Absorption Model

The excited state absorption model as developed by Huff and DeShazer[12] fits the saturation of many organic dyes very well. It is thus of use to review the essential points of that treatment here. Since the theory of the saturable resonator developed here involves only steady state solutions the review will be limited to that area.

In order to find the transmission of any material it is first necessary to find the intensity change over an incremental length of the material. In general this change is a function of intensity and is expressed in terms of the photon transport equation as

$$\frac{dI}{dZ} = - \sigma_1 N_0 \varepsilon(I) I \qquad (1)$$

where I is the photon flux density, (photons/cm^2 - sec), σ_1 is the absorption cross section (cm^2), N_0 is the

concentration of absorbing centers (number/cm^3), and $\varepsilon(I)$ is the saturation factor. The saturation factor expresses the fact that at finite intensities the number of ground state atoms are changing due to finite relaxation times from excited levels. Thus, as the intensity increases the population distribution of molecules in the different energy levels becomes non-thermal. Integration over the length L of the absorber yields the relation between the incident and transmitted photon flux densities

$$\int_{I_{in}}^{I_{out}} \frac{dI}{\varepsilon(I)I} = -\sigma_1 N_0 L = \ln T_0 \qquad (2)$$

where I_{in} is the incident photon flux density, I_{out} the transmitted flux density, and T_0 the transmittance in the limit of zero incident flux density. In order to restrict this discussion to the steady state case, the response time τ arising from the spontaneous decay rates of the saturable absorber material must be small with respect to the rate of change of the incident intensity. Another way of stating this is that if Δt is the full width at half maximum of the laser pulse then $\Delta t >> \tau$ implies that the steady state approximation is valid.

3. Energy Level Scheme for Organic Dyes

In order to find the form of $\varepsilon(I)$ it is first

necessary to start with some model of an energy level diagram, and with this it is possible to determine rate equations for the various levels. Then for any incident intensity it is possible to determine populations of the ground state and the various excited levels. A typical energy level diagram as given by Huff and DeShazer[12] is shown in Figure II.B.1. In this Figure the straight arrows indicate absorptions (if upward), or stimulated emissions (if downward). These transition rates are proportional to $\sigma_i I$ where σ_i is the absorption cross section for an absorption from the i^{th} state. The wiggly arrows indicate the spontaneous transition either radiative or non-radiative from state j to state i with corresponding rate A_{ji}.

The model for the organic dye consists of a singlet manifold and triplet manifold with the ground state of the singlet manifold being the ground state of the molecular system. Since Hund's rule seems to apply for molecules, the triplet state lies below the corresponding singlet state.[25,26] Thus the lowest lying excited state is the triplet state. In molecules the three states of the triplet level cannot usually be distinguished, thus each triplet level is 3-fold degenerate.[25] All states, however, are split into vibrational and rotational sublevels and are thermally populated. The transitions between these sublevels are thus very fast, making it

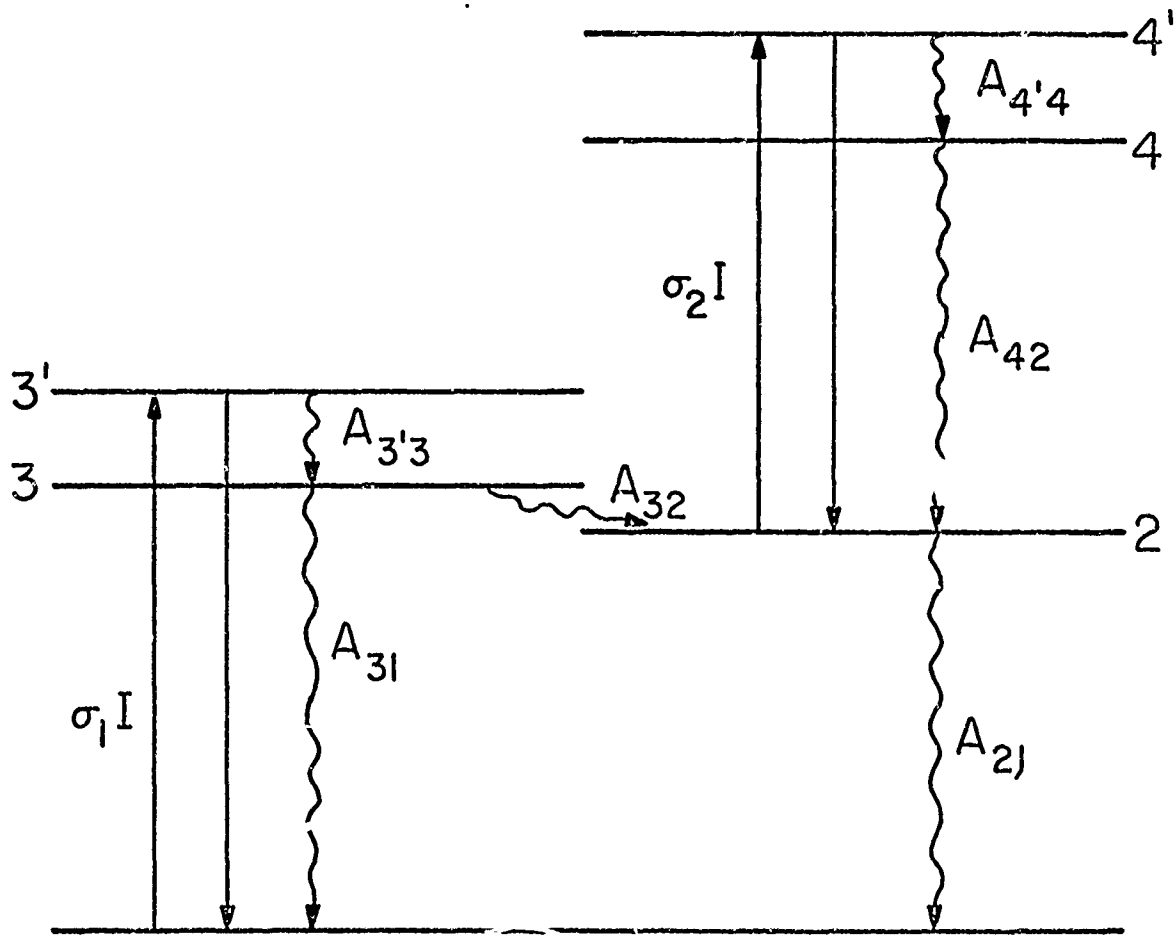

Figure II.B.1. Excited triplet state absorption energy level model from Huff and DeShazer (see reference 12).

necessary to consider only the sublevels (3') and (4'), respectively. Since singlet-triplet transitions are "forbidden" the cross section for absorption from the ground state singlet to the excited-state triplet is very small. This also holds for the transition from the excited singlet state to the lower triplet state, but due to a mechanism called intersystem crossing,[25,26] this rate can approach the singlet-singlet transition rates. Since the excited triplet to ground state (and excited state) singlet transition rates are relatively slow, the number of molecules in the triplet state can become appreciable.

There is then a hierarchy of transition rates, with the sublevel transition rates being the fastest, the transition rates between levels within a manifold and singlet to triplet transition rates being slower, and intermanifold triplet to singlet transition rates being the slowest. These relative rates will be used to make simplifying approximations later.

4. Excited State Absorption Model Saturation Equation

The photon transport equation for the model given in Figure II.B.1 is

$$\frac{dI}{dz} = - \sigma_1 N_0 \left[\frac{N_1 - N_{3'}}{N_0} + \frac{\sigma_2}{\sigma_1} \left(\frac{N_2 - N_{4'}}{N_0} \right) \right] I \, . \qquad (1)$$

The saturation parameter is then

$$\varepsilon(I) = \frac{N_1 - N_{3'}}{N_0} + \frac{\sigma_2}{\sigma_1}\left(\frac{N_2 - N_{4'}}{N_0}\right) \tag{2}$$

where N_i (i=1,2,3,3',4, or 4') is the population density of the i^{th} state and N_0 is the total molecular concentration. It can be assumed that $N_0 = N_1+N_2+N_3+N_{3'}+N_4+N_{4'}$.

For steady state, $dN_i/dt = 0$,

where N_i is again the population of the i^{th} level. The following result for the saturation parameter is then obtained

$$\varepsilon(\bar{I}) = \frac{1 + K_1\bar{I} + K_3\bar{I}^2}{1 + K_2\bar{I}} \tag{3}$$

where $\bar{I} = \sigma_1 tI$ is a dimensionless flux, $t = (A_{31} + A_{32})^{-1}$ and

$$K_1 = 1 + \frac{A_{32}}{A_{21}} + 2\left(\frac{A_{31} + A_{32}}{A_{3'3}}\right) \tag{4}$$

$$K_2 = \frac{\sigma_2}{\sigma_1}\left|\frac{A_{32}}{A_{21}} + \frac{A_{42}}{A_{4'4}}\left(\frac{A_{31} + A_{32}}{A_{42}}\right)\right| \tag{4}$$

$$K_3 = \frac{\sigma_2}{\sigma_1}\left(\frac{A_{31}+A_{32}}{A_{42}}\right)\left[\frac{A_{42}}{A_{4'4}}\left\{1 + 2\frac{A_{32}}{A_{21}} + 2\left(\frac{A_{31}+A_{32}}{A_{3'3}}\right)\right\} + \frac{A_{32}}{A_{21}}\right] \quad (4)$$

Upon integration of equation 1, using equation 3, the following result is obtained (see Ref. 12),

$$\ln \frac{T}{T_0} = C_1 \ln\left[\frac{1 + C_2\bar{I}_{in}}{1 + C_2 T\bar{I}_{in}}\right] + C_3\bar{I}_{in}(1-T) \quad (5)$$

where $$C_1 = (K_1K_2-K_3)/K_2^2 - 1 \quad (6)$$

$$C_2 = K_2 \quad (6)$$

$$C_3 = K_3/K_2 \, . \quad (6)$$

Since levels 3 and 3' are vibronic substates, the transitions between them are fast. Thus, the following approximation can be made, i.e.,

$$A_{3'3} >> A_{31} + A_{32}.$$

The same is true of levels 4 and 4', thus $A_{4'4} >> A_{42}$.

Using these approximations in equations 6, the following approximations can then be made

$$C_1 \approx \left[(1 + \gamma - \zeta)/\sigma_{21}\gamma\right] - 1$$

$$C_2 \approx \sigma_{21}\gamma \qquad (7)$$

$$C_3 \approx \zeta$$

where $\gamma = A_{32}/A_{21}$, $\sigma_{21} = \sigma_2/\sigma_1$, and $\zeta = (A_{31}+A_{32})/A_{42}$.

5. Residual Absorption Model

For many cases[12,15] $C_3 \to 0$ and therefore the saturation behavior is dependent on only two parameters C_1 and C_2. C_1 determines the residual absorption as well as having a large effect on the shape of the transmission versus intensity curve. The residual absorption $(1 - T_f)$ can be obtained by letting $I_{in} \to \infty$ in equation (5). Then

$$\ln T_f = \left(\frac{1}{1+C_1}\right) \ln T_0 \qquad (1)$$

where T_f is the transmission when $I_{in} \to \infty$. It is seen here that for $T_f=1$, $C_1 \to \infty$. Now using the above approximations in equation (5), it is possible to solve I_{in} as a function

of T. This gives the following result

$$I_{in} = B_2 \left| \frac{(T/T_0)^{B1} - 1}{1 - T(T/T_0)^{B_1}} \right| \qquad (2)$$

where $B_2 = \frac{1}{\sigma_1 + C_2}$ and $B_1 = 1/C_1$.

Since $C_3 \to 0$ equations (7) of the previous section become

$$C_1 = \frac{1 + A_{32}/A_{21}}{\sigma_{21} A_{32}/A_{21}} - 1 \qquad (3)$$

and

$$C_2 = \sigma_{21} \frac{A_{32}}{A_{21}} \qquad (3)$$

6. Justification of Excited State Absorption Model

In this section it will be shown why the excited state absorption model used the triplet-triplet transition for excited state absorption. Figure II.B.2 shows a typical energy level diagram for a molecular system with both singlet and triplet excited state absorptions.[25,26] In this diagram, levels 1, 3, and 5 are singlet levels while levels 2 and 4 are triplet levels. The primed number levels are the vibrational or rotational sublevels of the

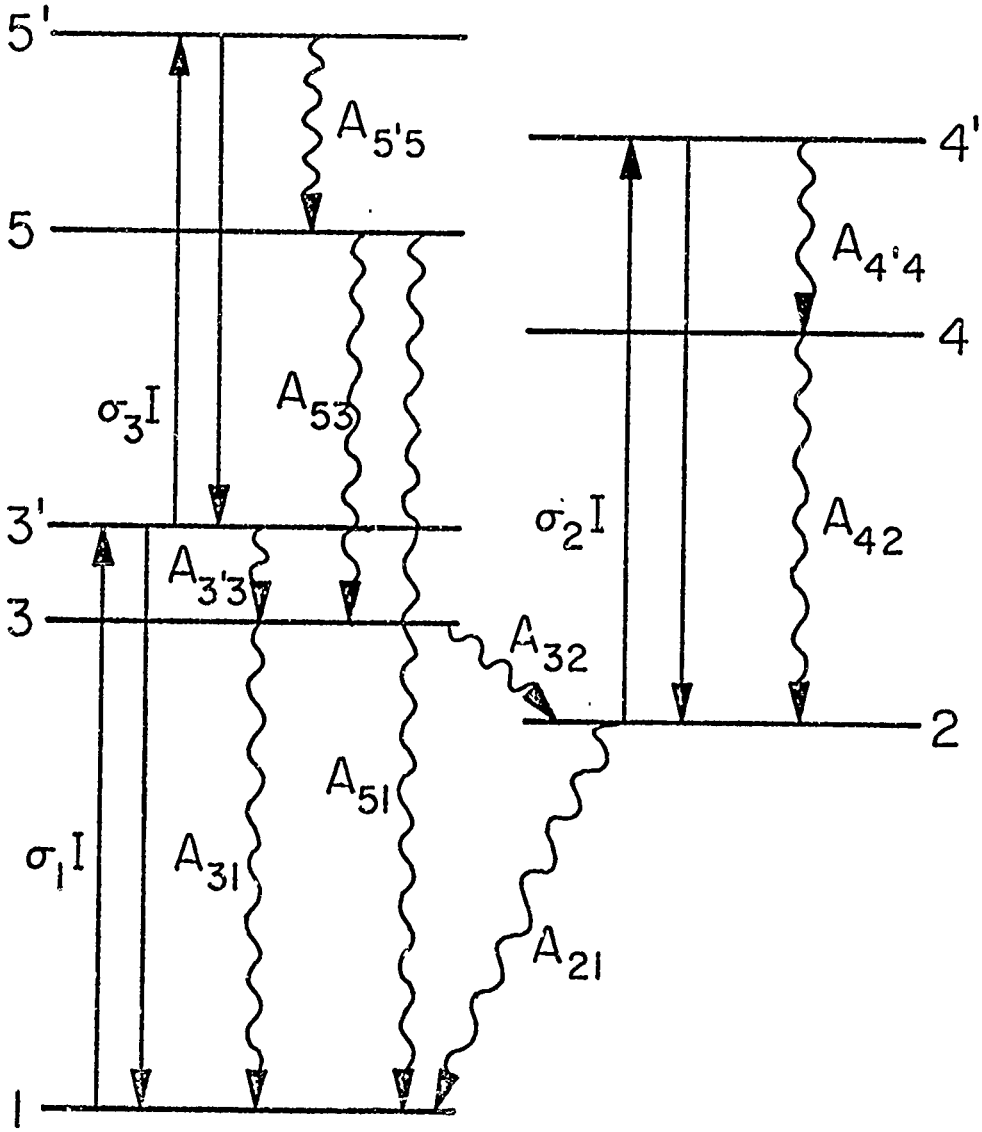

Figure II.B.2. Energy level diagram for both excited singlet state and excited triplet state absorption.

respective levels. It is then possible as before, to solve the rate equations in steady state and obtain the population of each level as a function of the intensity.

The photon flux equation for this model is

$$\frac{dI}{dZ} = -\sigma_1 N_0 \left[\frac{N_1 - N_3'}{N_0} + \frac{\sigma_2}{\sigma_1} \frac{N_2 - N_4'}{N_0} + \frac{\sigma_3}{\sigma_1} \frac{N_3 - N_5'}{N_0} \right] I$$

The saturation parameter is then

$$\epsilon(I) = \frac{N_1 - N_3'}{N_0} + \frac{\sigma_2}{\sigma_1} \frac{N_2 - N_4'}{N_0} + \frac{\sigma_3}{\sigma_1} \frac{N_3 - N_5'}{N_0}$$

The population densities are given in terms of intensities by solving the rate equations. Thus, in steady state

$$\epsilon(I) = \frac{1 + K_1 I + K_2 I^2}{1 + K_3 I + K_4 I^2 + K_5 I^3}$$

where $$K_1 = \sigma_3 \left[\frac{2}{A_1} - \frac{A_{53}}{A_1 A_2} - \frac{1}{A_{5'5}} \right] + \sigma_2 \left[\frac{A_3}{A_1} + \frac{1}{A_{4'4}} \right]$$

$$K_2 = \sigma_2 \sigma_3 \left[\frac{2}{A_1 A_{4'4}} + \frac{A_3}{A_1 A_{5'5}} + \frac{1}{A_{4'4} A_{5'5}} - \frac{A_{53}}{A_1 A_2 A_{4'4}} \right]$$

$$K_3 = \sigma_3 \left[\frac{1}{A_{5'5}} + \frac{1}{A_1} - \frac{A_{53}}{A_1 A_2} + \frac{1}{A_{4'4}}\right] + \sigma_1\left[\frac{2}{A_{3'3}} + \frac{A_3+1}{A_1}\right]$$

$$K_4 = \sigma_2\sigma_3\left[\frac{1}{A_{4'4}A_{5'5}} + \frac{1}{A_1 A_{4'4}} - \frac{A_{53}}{A_1 A_2 A_{4'4}} + \frac{1}{A_1 A_2}\right.$$

$$\left. + \frac{1}{A_1 A_{5'5}}\right] + \sigma_1\sigma_3\left[\frac{2}{A_{3'3}A_{5'5}} + \frac{1}{A_1 A_{4'4}}\right.$$

$$\left. - \frac{2A_{53}}{A_1 A_2 A_{3'3}} + \frac{2(A_3+1)}{A_1 A_{5'5}}\right] + \sigma_1\sigma_2\left[\frac{2}{A_{3'3}A_{4'4}}\right.$$

$$\left. + \frac{A_3}{A_1 A_{42}} + \frac{A_3}{A_1 A_{4'4}}\right]$$

$$K_5 = \frac{\sigma_1\sigma_2\sigma_3}{A_1 A_{4'4} A_{5'5}}\left[\frac{2(A_1 + A_{5'5})}{A_{3'3}} - \frac{2A_{53}A_{5'5}}{A_2 A_{3'3}}\right.$$

$$\left. + 2(A_3 + 1) + \frac{A_3}{A_{42}} A_{4'4} + \frac{A_{5'5}}{A_2}\right]$$

$$A_1 = A_{32} + A_{21}$$

$$A_2 = A_{51} + A_{53}$$

and $A_3 = A_{32}/A_{21}$.

Since the vibronic sublevel transitions are very fast, the rates $A_{3,3}$, $A_{4,4}$, and $A_{5,5}$ can be assumed to be infinite. This assumption yields

$$K_1 = \sigma_3\left(\frac{2}{A_1} - \frac{A_{53}}{A_1A_2}\right) + \sigma_2\frac{A_3}{A_1}$$

$$K_2 = 0$$

$$K_3 = \sigma_3\left(\frac{1}{A_1} - \frac{A_{53}}{A_1A_2}\right) + \sigma_1\frac{A_3+1}{A_1}$$

$$K_4 = \frac{\sigma_2\sigma_3}{A_1A_2} + \frac{\sigma_1\sigma_2A_3}{A_1A_{42}}$$

$$K_5 = 0$$

But for many organic dye systems $A_3 \sim 10^4$ and $A_{51} \sim A_{53} \sim A_{42}$[25], so terms including A_3 can be assumed to be much larger than the others.

Inspection of the above equations shows that it is possible to ignore the terms involving σ_3 and thus the excited singlet level absorption is small. By ignoring σ_3

the results of the preceding section are obtained. For phthalocyanines, Hercher[13] has shown that the excited singlet state absorption is an important effect. This is reasonable if in phthalocyanines the rate A_{32} is much slower than for cryptocyanine and A_3 is much smaller so σ_3 terms cannot be neglected. It has been shown that A_{31} is much smaller for phthalocyanines,[13] however A_{32} has not been measured. Therefore excited singlet state absorption can be important for phthalocyanine dyes. The time range for making steady state approximations will, of course, be different for phthalocyanine.

7. Solvent Effects.

It will be shown that the saturable resonator performance improves by decreasing B_1 (see equation II.B.-5.2). This, of course, means reducing the residual absorption of the saturable absorber. There are several quantities, namely the decay rate A_{21} and the cross sections σ_1 and σ_2, which can be changed by changing the solvent in which the dye is dissolved. Changes in these quantities in turn alter the B_1value.

Bayliss[27] has shown that the shift of the absorption spectra of solute molecules in a dielectric solvent medium is related to the index of refraction of the solvent. This result has been experimentally verified for several

cyanine dyes.[28] The following relationship gives the shift,

$$\Delta\nu(cm^{-1}) = (const)\ (f/\nu\alpha)\ \frac{n^2 - 1}{2n^2 + 1} \qquad (1)$$

where const = 10.7×10^9 cm, f is the oscillator strength, α is the polarizability in units of cm^3, n the index of refraction of the solvent, and ν is in cm^{-1}. This frequency shift causes a change in the cross section for a given frequency. This may then be possible to alter the excited state absorption.

Since the level 2 is a triplet level and the level 1 is a singlet level (see Figure II.B.2) transitions $2 \rightarrow 1$ are "forbidden", making the radiative lifetime very long. If $A_{32} >> A_{21}$, there is a "bottleneck" which causes a large residual absorption to occur. Thus, if nonradiative decay rates ($2 \rightarrow 1$) can be increased, the residual absorption will be reduced. One way to increase this decay rate is to introduce a paramagnetic substance such as molecular oxygen.[21,25,26,29,30] This paramagnetic substance necessarily has a ground state in which the total spin is non-zero. A paramagnetic substance can magnetically couple to the triplet state of the solute molecule during a collision. This removes energy from the excited triplet state of the dye molecule by transfering

it to the paramagnetic molecule. The nonradiative decay rate of the triplet-singlet transition is thus related to the collision rates between the paramagnetic (O_2) molecules and the dye molecules in the excited triplet state. This collision rate will depend on the concentration of paramagnetic molecules and the viscosity of the solvent. Thus with increasing O_2 concentration the triplet-singlet decay rate will increase. The viscosity enters the collision rate through the mobility of the solute molecules (both dye and paramagnetic molecules). Frenkel[31] shows that the mobility is inversely proportional to the viscosity. For the simplified case of spherical particles this is given by

$$\alpha = \frac{1}{6\pi a\mu} \qquad (2)$$

where α is the mobility, μ is the viscosity, and a is the radius of a particle in the liquid. Since the collision rate is directly proportional to the mobility then the collision rate is inversely proportional to the viscosity. It is then desirable to reduce the viscosity in order to decrease residual absorption. At the same time the solubility of the paramagnetic substance should be high. Porter *et. al.*[32] have shown the effect of O_2 concentration on the triplet state.

8. Semiconductor Glass Saturable Absorbers

The semiconductor glass saturable absorbers consist of semiconductor material crystallites in a glass host. The compound used is Cd: Se: S made from a mixture CdS and CdSe. By adjusting concentrations of CdS and CdSe together with a heat treating process, Litton Industries has been able to adjust the band gap between the valence and conduction bands to be slightly smaller than the energy of a photon with wavelength $\lambda = 6943$ Å (ruby). The two bands are very nearly parabolic.

Figure II.B.3 gives an energy diagram in $\vec{k}$ space.[33] E_g is the band gap and E_L the energy in a laser photon. Without incident light and if $E_g >> kT$ then most electrons are in the valence band. However, for each laser photon absorbed an electron is excited into the conduction band forming an electron-hole pair. With an increasing number of incident photons, many electrons can be excited into the conduction band, thus shifting the absorption edge to shorter wavelengths and increasing the transmission at the laser wavelength.

Decay of the electrons from the conduction band, of course, is due to the recombination of the electron-hole pairs. With impurities present this decay rate can be quite high. However, these impurities can also be responsible for unsaturable losses such as scattering. Residual

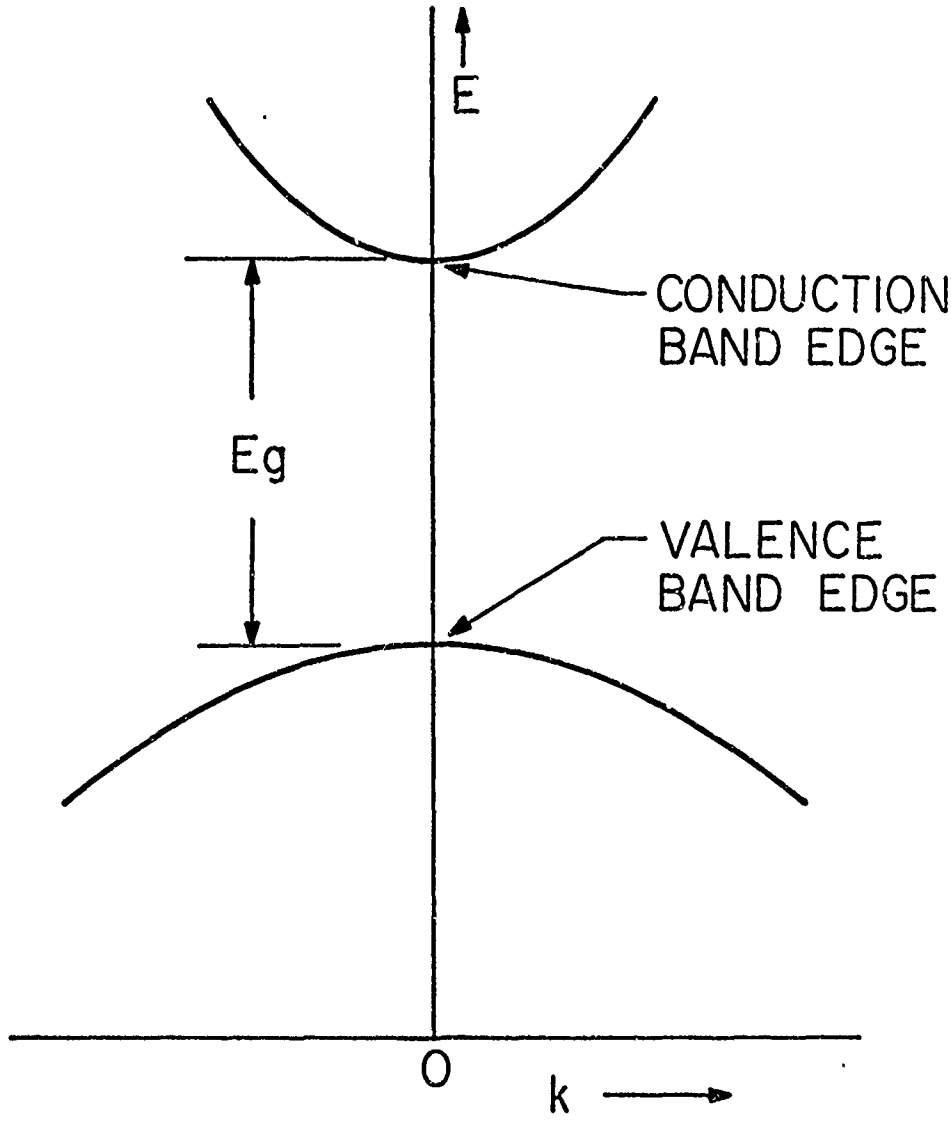

Figure II.B.3. Band structure in k-space for semiconductor saturable absorber.

absorption by conduction band electrons should be small since this absorption involves indirect transitions and these transitions are highly improbable. Therefore, the single absorption model with unsaturable loss is developed.

9. Single absorption with Unsaturable Loss

An energy level diagram for the model of single absorption with an unsaturable loss is given in Figure II.-B.4. This model is picked for the semi-conductor saturable absorber because the transition causing the absorption is due to an interband transition, and this can be approximated by a two level system under 2 conditions; (1) the laser photon energy is close to the band gap energy; and (2) the two levels are actually two distributions of energy levels. The band gap, E_g corresponding to the separation of levels 1 and 2, is slightly smaller than the energy of the laser photon. With no incident field the conduction band is unpopulated except for a small number of electrons due to the Fermi-Dirac distribution and thus the valence band is considered completely filled. If E_g is the band gap and E_L the photon energy, then electrons to a depth $\Delta E = E_L - E_g$ into the valence or band, can be excited into the conduction band. The unsaturable loss is assumed to be from impurities or scattering and appears unsaturable.

If the relaxation rates are much faster than the time variation of the pulse, the steady state approximation

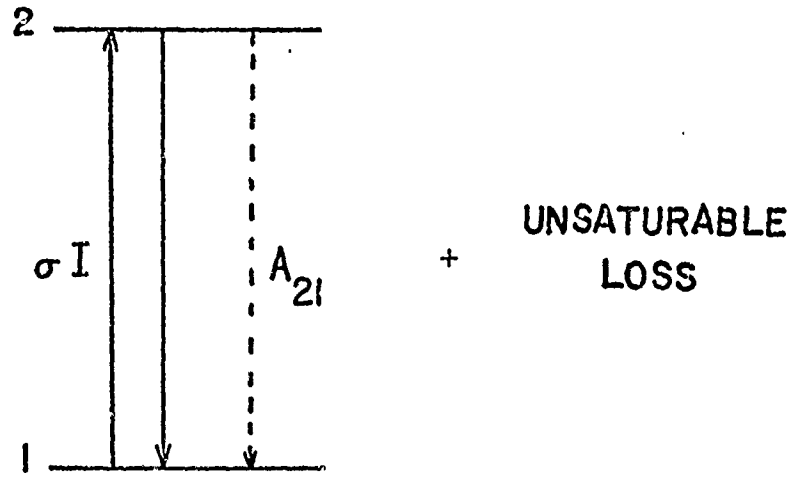

Figure II.B.4. Energy level diagram for single absorption with unsaturable loss.

can again be used. The photon flux equation for this model is

$$\frac{dI}{dZ} = -\sigma_1(N_1 - N_2)I - \alpha I \qquad (1)$$

where N_1 is the population of the lower level, N_2 is the population in the upper level, and $\alpha = \sigma_L N_L$ where N_L is the impurity concnetration. Now $N_0 = N_1 + N_2$ is the total number of electrons available for interaction with the light, and since $E_g >> kT$ at room temperature, then for zero input $N_0 \approx N_1$. By knowing the density of states in the valence band and value of ΔE it is possible to find N_0. From the two level model the following rate equations are obtained

$$\frac{dN_1}{dt} = -\sigma_1 N_1 I + \sigma_1 N_2 I + A_{21} N_2 \qquad (2)$$

$$\frac{dN_2}{dt} = \sigma_1 N_1 I - \sigma_1 N_2 I + A_{21} N_2 \ . \qquad (3)$$

For steady state conditions

$$\frac{dN_1}{dt} = \frac{dN_2}{dt} = 0$$

thus $$\frac{N_1 - N_2}{N_0} = \frac{1}{\frac{2\sigma_1 I}{A_{21}} + 1} . \qquad (4)$$

Putting this into the photon transport equation and integrating over the length of the absorber (L) finally yields the equation

$$\ln\left(\frac{T}{T_0}\right) = \beta/\alpha \ln\left[\frac{\beta/\alpha + 1 + 2\bar{I}_{in}}{\beta/\alpha + 1 + 2T\bar{I}_{in}}\right] \qquad (5)$$

where $\beta = \sigma_1 N_0$, $\bar{I} = \frac{\sigma_1 I}{A_{21}}$, and I is the photon flux density.

In the limit as $I_{in} \to \infty$, $T \to T_f$. Taking this limit in equation (5) gives

$$\ln T_f = \frac{1}{1 + \beta/\alpha} \ln T_0 . \qquad (6)$$

For $\beta/\alpha \to \infty$, $T_f = 1$ as would be expected since this would mean $\alpha \to 0$.

Solving for I_{in} in terms of T in equation (5) gives

$$I_{in} = C_2 \left[\frac{(T/T_0)^{C_1} - 1}{1 - T(T/T_0)^{C_1}}\right] \qquad (7)$$

where the parameter $C_1 = \alpha/\beta$ can be obtained from T_f with equation (6) and $C_2 = (A_{21}/2\sigma_1)(\beta/\alpha + 1)$ can be obtained knowing C_1 and fitting equation (7) to the data. Thus C_1 is a measure of the residual absorption and C_2 a measure of the intensity range of saturation.

10. General Parametrization of Saturable Absorbers

It has been shown in Sections II.B.5 and II.B.8 that the excited state and single absorption models have the same functional dependence of intensity on transmission. This is given by

$$I_{in} = D_2\left[\frac{(T/T_0)^{D_1} - 1}{1 - T(T/T_0)^{D_1}}\right] \tag{1}$$

where I_{in} is the incident intensity in terms of watts/cm^2. The conversion between this intensity and the photon flux density used in the preceding derivations is $I_{in} = h\nu \times$ (photon flux density), h is Planck's constant and ν the frequency of the light. For 6943A, $h\nu = 2.86 \times 10^{-19}$ joules.

Figure II.B.5 shows the variation of equation (1) for different values of D_1. Not only does D_1 change the value of the final transmission T_f, but it also changes the range of intensities over which the largest transmission

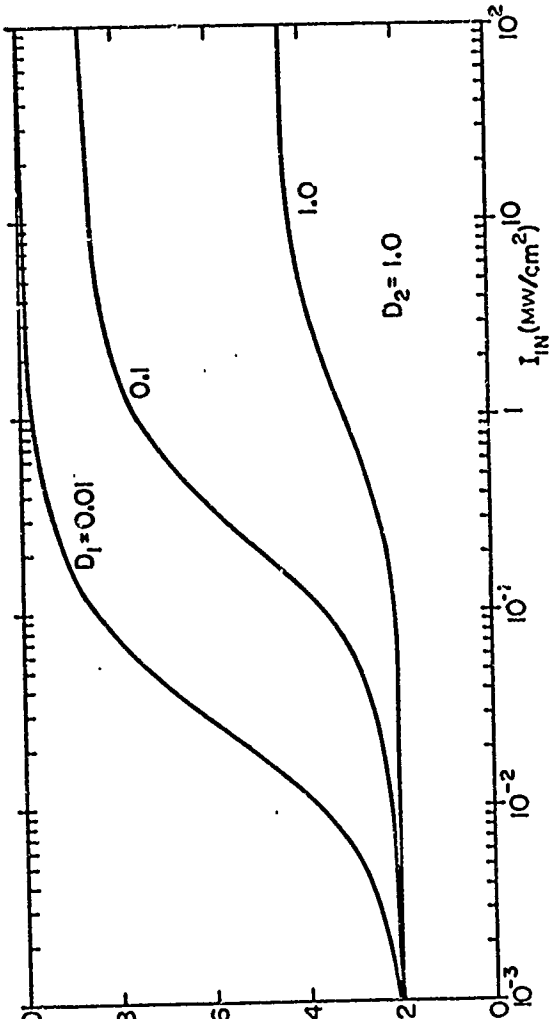

Figure II.B.5. Plot of the saturation equation for several values of D_1.

change occurs since the maximum slope also increases with decreasing D_1.

In Figure II.B.6 equation (1) is shown for different values of the parameter D_2. It is seen that changing D_2 does not affect the shape of the curve but does change the position of the curve along the intensity axis. Thus by picking a D_1 value to fit the measured saturation of an absorber, the D_2 value can be altered to fit the intensity range.

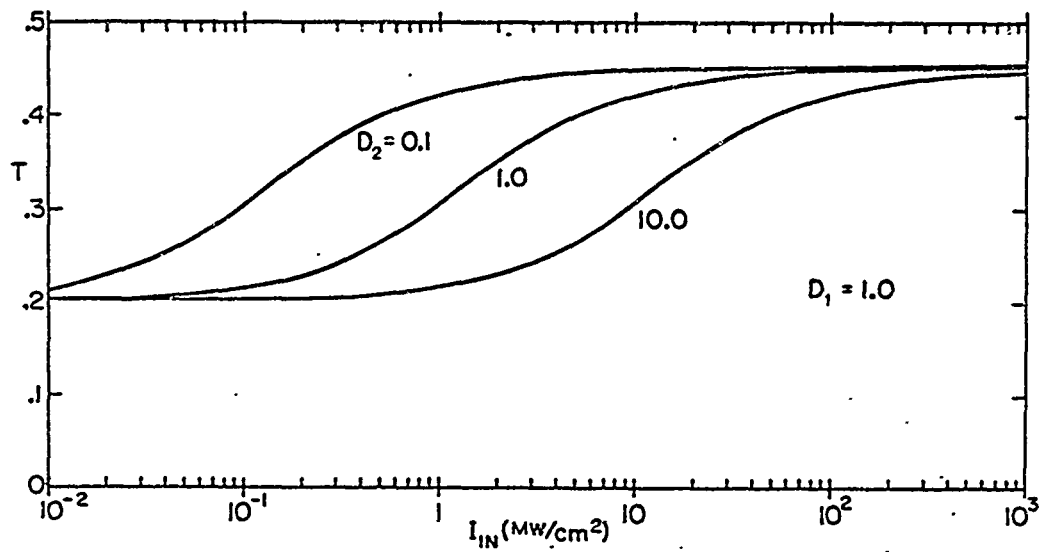

Figure II.B.6. Plot of the saturation equation for various values of D_2.

C. Fabry-Perot Interferometer with a Saturable Absorber

1. Coupling of the Fabry-Perot Interferometer with the Saturable Absorber.

With a model of the saturable absorber now determined it is possible to solve the complete problem of the saturable resonator. The saturable absorber model gives the intensity dependence of the transmission for a single incident beam. However when the saturable absorber is put between the two reflectors there are actually two beams incident on the absorber. These beams are comprised of the two waves traveling in opposite directions between the mirrors. These beams maintain the transmission at a certain level and it is necessary to find an effective incident beam which can be used in the relations derived for the saturable absorber. This is an approximation since it is really a standing wave which is interacting with the absorber, not a traveling wave.

To obtain this effective intensity, first let the intensity (I_i) incident on the saturable resonator be such that the single pass transmission of the absorber is T_α (see Figure II.C.1). Let I_+ be the sum of all waves traveling in the direction of the incident beam at the inner surface of reflector 1. Let I_- be the sum of all waves traveling in the opposite direction of the incident beam and at the inner surface of reflector 2. Here, for

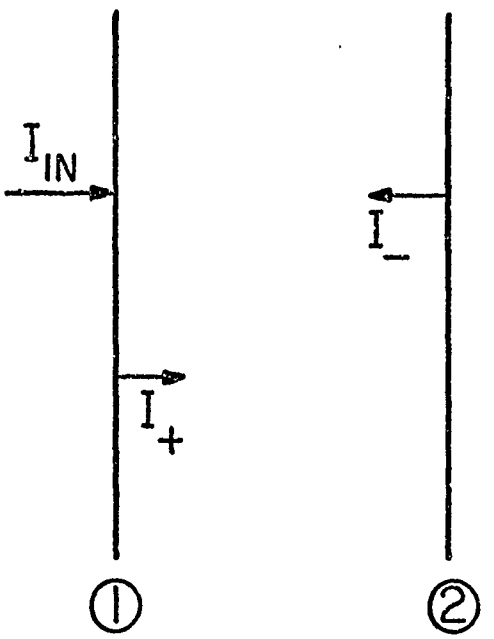

Figure II.C.1. The standing wave in the cavity results from the two traveling waves I_+ and I_-.

simplicity it is assumed the wavelength of the incident intensity matches the resonance of the interferometer. The following relations must then hold,

$$I_+(1 - T_\alpha) = I_{+\ abs} \tag{1}$$

$$I_-(1 - T_\alpha) = I_{-\ abs} \tag{2}$$

where $I_{\pm\ abs}$ are the intensities absorbed from the respective beams. The total intensity absorbed is then

$$I_A = I_{+\ abs} + I_{-\ abs}$$

$$= (1 - T_\alpha)(I_+ + I_-) \quad . \tag{3}$$

But for steady state conditions the following is true

$$I_- = T_\alpha R I_+ \tag{4}$$

where R is the reflectivity of a single mirror. Substituting this into equation (3) gives

$$I_+(1 - T_\alpha)(1 + T_\alpha R) = I_A \ . \tag{5}$$

The effective intensity (I_{eff}) is defined to be such that

$$I_{eff}(1 - T_\alpha) = I_A.$$

Therefore

$$I_{eff} = I_+ (1 + T_\alpha R).$$

It is now easy to relate I_+ to I_i from the results of Section II.A, giving

$$I_+ = \frac{I_i(1 - R)}{(1-T_\alpha R)^2 + 4RT_\alpha \sin^2\delta/2} \tag{6}$$

From the solution of the saturable absorber problem it is seen that I_{eff} can be algebraically expressed solely as a function of the transmission, but that the transmission cannot be expressed solely as a function of intensity. This means I_{eff} must be given in terms of transmission, but from Section II.A, the ratios I_R/I_i, I_T/I_i, and I_A/I_i are also given as functions of transmission. Thus, in order to get I_R, I_T, or I_A as functions only of the incident intensity, it is necessary to solve two relations simultaneously. This is done by first calculating the ratio I_N/I_i (N = R,T, or A) for some T_α

from equations 6, 7, and 13, of Section II.A.3. Next I_{eff} is calculated for the corresponding T_α. Finally I_i is obtained which is used to get I_N. It was shown in the saturable absorber section, II.B, that

$$I_{eff} = D_2 \frac{(T_\alpha/T_0)^{D_1} - 1}{1 - T_\alpha(T_\alpha/T_0)^{D_1}} \tag{7}$$

This gives the following value for I_i

$$I_i = \left[\frac{(1-T_\alpha R)^2 + 4RT_\alpha \sin^2\delta/2}{(1-R)(1+T_\alpha R)}\right]\left[D_2\left\{\frac{(T_\alpha/T_0)^{D_1} - 1}{1-T_\alpha(T_\alpha/T_0)^{D_1}}\right\}\right] \tag{8}$$

It should be remembered that T_α has the limits $T_0 \leq T \leq T_f$ where T_0 and T_f were defined in the saturable absorber section.

2. Properties

Using the above relations for I_T vs I_i, the curves in Figure II.C.2 are obtained for the resonant case ($\delta=2m\pi$). There are several important results shown in these curves. The first thing to be noted is that the parameter D_2 has the same property as for the saturable absorber alone, that is, it is an intensity scaling factor. This means that D_2 does not affect the character of the

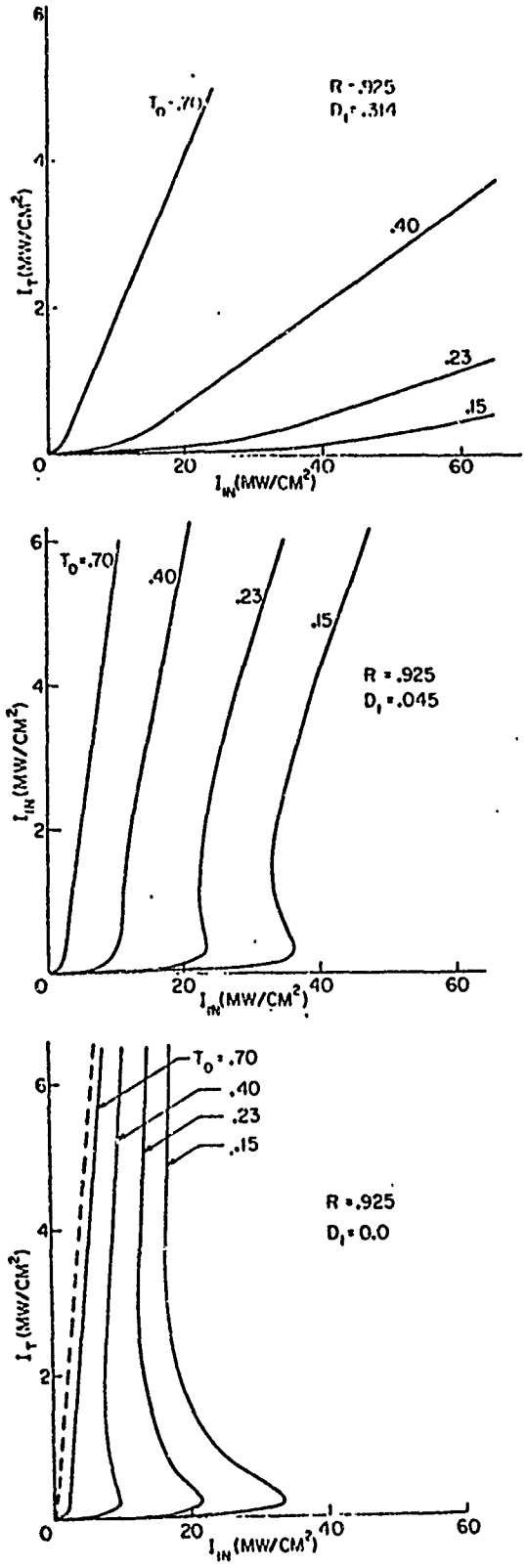

Figure II.C.2. Input versus output of the saturable resonator for different values of R, T_0, and D_1.

curves but only the absolute intensity range at which they change. For the following discussion, the D_2 parameter is not of importance. The features of all the curves are therefore determined by the remaining parameters T_0, R, and D_1. T_0 and D_1 determine the value of T_f and since the transmission of the saturable resonator is due in part to the absorber transmission, then T_f gives the maximum transmission as $I_i \to \infty$. Thus, as $I_i \to \infty$

$$\frac{I_T}{I_i} = \frac{(1-R)^2 T_f}{(1-RT_f)^2}$$

and this is the final slope which all the curves must approach for high intensities. T_f decreases with decreasing T_0 or D_1 so the maximum transmission of the resonator is determined by these two parameters for any specific value of R.

The most important property to be observed in Figure II.C.2 is that for certain values of T_0 and D_1, I_T is triple valued over a limited range of I_i values. This gives a bistable character to the saturable resonator. To see this, it is only necessary to watch the output intensity with variation of the incident intensity. As I_i increases to the value I_{i_1} (see Figure II.C.3), I_T increases approximately linearly, and approaches the limiting value

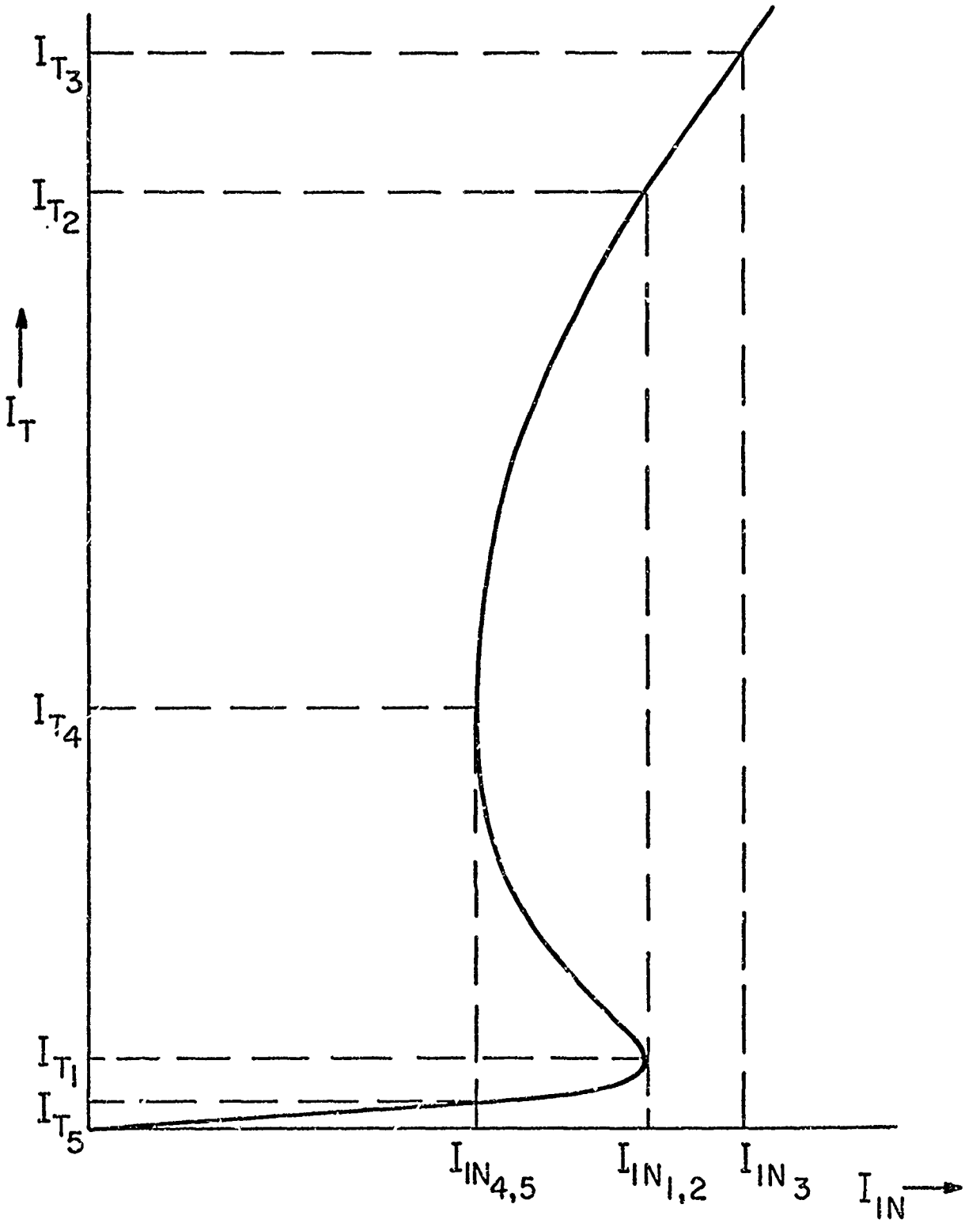

Figure II.C.3. Illustration of bistable operation and the optical hysteresis loop.

I_{T_1}. At $I_i = I_{i_1}$, however, I_T suddenly jumps discontinuously from I_{T_1} to I_{T_2}. There is a corresponding discontinuous increase in transmission from a rather low value to the higher value. The saturable resonator thus has a bistable-like operation since there are two widely separated ranges of transmission at which the resonator operates, and the state of the transmission depends on the incident intensity. With a further increase of I_i, I_T again continues to increase almost linearly but with a different slope. Now when I_i begins to decrease, I_T also decreases, but there is not a discontinuous jump until I_i reaches I_{i_4} ($I_{i_4} < I_{i_2}$) at which point I_T discontinuously drops from I_{T_4} to I_{T_5}. Thus, the I_T vs I_i curve also has a hysteresis loop besides the bistable character. It should be stressed again at this point that these results are derived assuming a steady state condition and the hysteresis is not a time dependent effect of the saturable absorber alone.

3. Criteria for Bistable Operation

It is possible to establish criteria for operating a saturable resonator in the bistable regime. This is accomplished by determining whether or not the slope of the I_i vs I_T curve has a zero for a specific set of values of R, T and D_1. If it does, this implies bistable operation is possible. The range of values of R, T_0 and D_1 giving

bistable operation determine the bistable operation region in (R, T_0, D_1) space. The slope (dI_i/dI_T) is obtained by solving equation (7), Section II.A.3 for I_i. However, since it is only the zero value of the slope that is desired, it is easier to find the quantity (dI_i/dI_+) and determine its zero values. The zero values of this then give zero values for (dI_i/dI_T) since

$$\frac{dI_i}{dI_T} = \frac{dI_i}{dI_+}\frac{dI_+}{dI_T} \tag{1}$$

The derivative (dI_i/dI_+) can be obtained from equation (6) of Section II.C.1. Taking the derivative gives

$$\frac{dI_i}{dI_+} = \frac{(1-T_\alpha R)^2 + 4RT_\alpha \sin^2\delta/2}{1-R^2} + \frac{I_+}{(1-R)}\left[-2R(1-RT_\alpha) + 4R\sin^2\delta/2\right]\frac{dT_\alpha}{dI_+} . \tag{2}$$

The term (dT_α/dI_+) can be evaluated from

$$I_+ = (1 + RT_\alpha)^{-1} I_{eff} .$$

Using the expression for I_{eff}, then

$$\frac{dI_+}{dT_\alpha} = \frac{D_2}{1+RT_\alpha}\left[\frac{-R}{1+RT_\alpha}\left[\frac{(T_\alpha/T_0)^{D_1}-1}{1-T_\alpha(T_\alpha/T_0)^{D_1}}\right]\right.$$

$$+\frac{(D_1/T_0)(T_\alpha/T_0)^{D_1-1}[1-T_\alpha(T_\alpha/T_0)^{D_1}]}{[1-T_\alpha(T_\alpha/T_0)^{D_1}]^2}$$

$$\left.+\frac{[(T_\alpha/T_0)^{D_1}-1](D_1+1)(T_\alpha/T_0)^{D_1}}{[1-T_\alpha(T_\alpha/T_0)^{D_1}]^2}\right]. \qquad (3)$$

If $$\frac{dI_+}{dT_\alpha} \neq 0$$

then $$\frac{dT_\alpha}{dI_+} = \left(\frac{dI_+}{dT_\alpha}\right)^{-1} \qquad (4)$$

so equation (3) can be substituted into equation (2) and by varying T_α over the range T_0 to T_f for a set of R, T_0 and D_1, zero values are searched for. This variation of T_α corresponds indirectly to a variation of the incident intensity. If there is a zero for a specific R, T_0, and D_1, then the saturable resonator can operate bistably and is said to lie in the bistable region. Since this region is dependent on the three variables R, T_0, and D_1, it is

separated from the region of normal operation by a 3-dimensional surface in (R, T_0, D_1) space. Projections of this surface onto the $1/D_1$, T_0 plane and $1/D_1$, R plane are shown in Figures II.C.4 and II.C.5. It is now possible to predict which saturable absorbers, characterized by equation (1) of Section II.B.10 give bistable operation, the ranges of R and T_0 which are needed as well as the intensity required for any saturable absorber lying in the bistable region to operate bistably.

4. Pulse Shaping

Figures II.C.6 shows a transfer curve for the transmission of a laser pulse (with Gaussian time dependence) by the saturable resonator. The figure is for the case in which the saturable absorber operates in the bistable region. For a given peak intensity and a specific dye system the intensity level (I_0) at which the saturable resonator turns "on", can be adjusted by varying mirror reflectivity and/or low level absorber transmission. By doing this the amount of pulse narrowing can be controlled.

The case picked for illustration in Figure II.C.6 is for I_0 slightly less than the peak intensity of the incident pulse (I_p). The incident pulse has a FWHM of Δt. Here the pulse narrowing is very prominent. An important thing to notice is that the transmitted pulse shows an

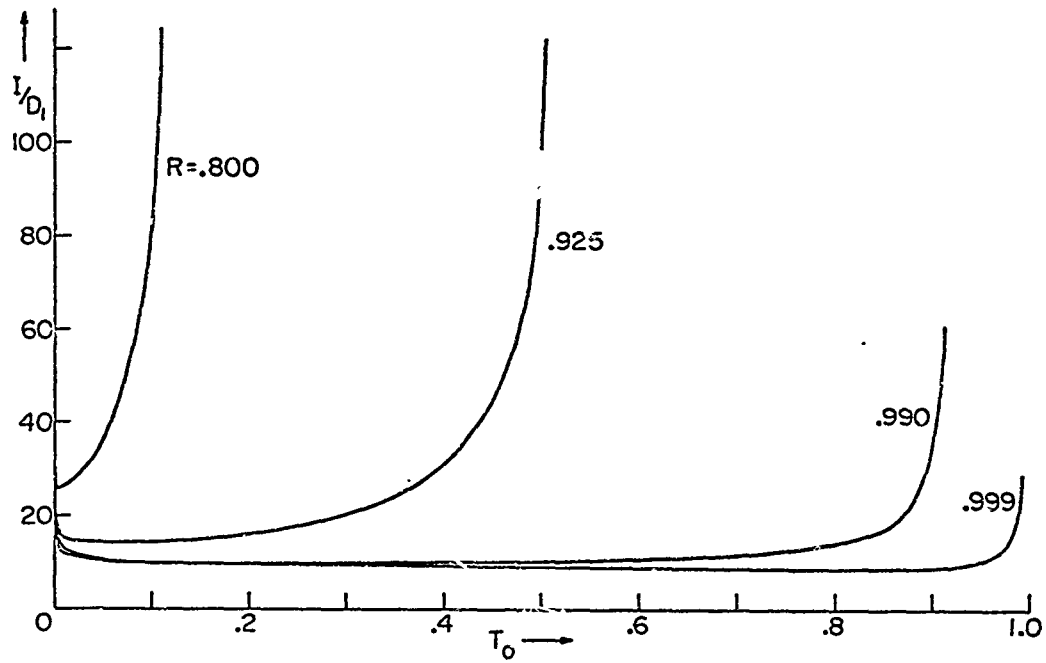

Figure II.C.4. Bistable criteria for T_0 vs $1/D_1$ and various R. The region above each curve corresponds to bistable region.

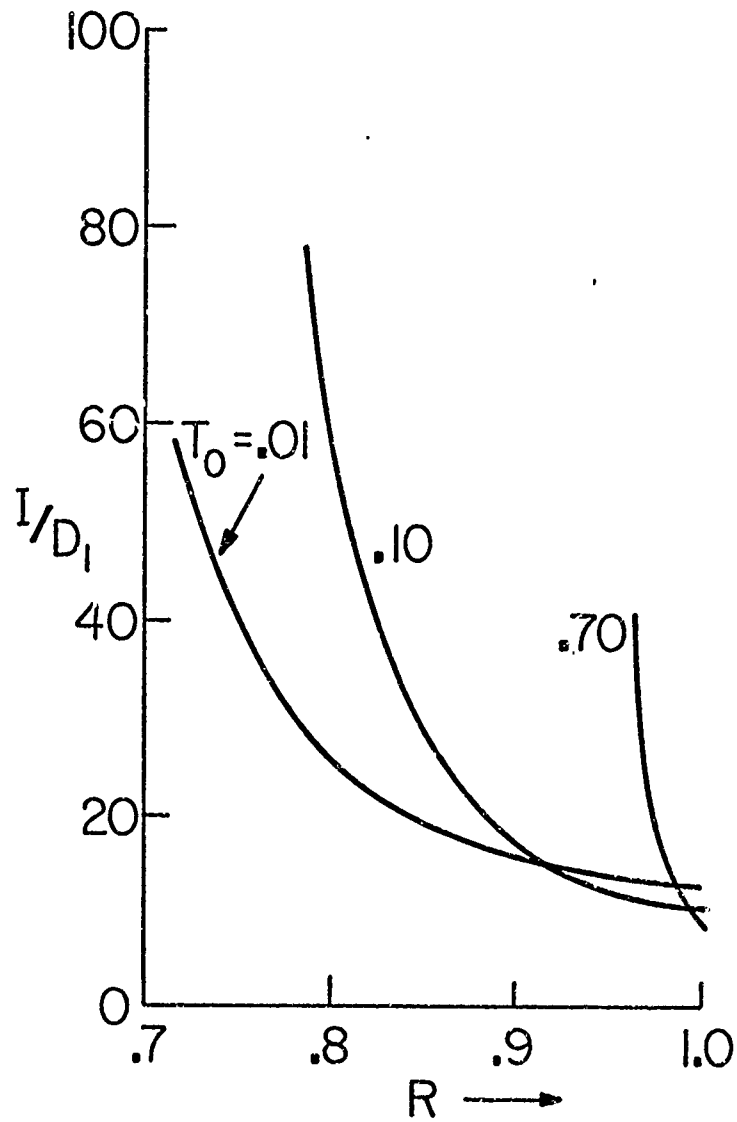

Figure II.C.5. Bistable criteria for R vs $1/D_1$ and various T_0.

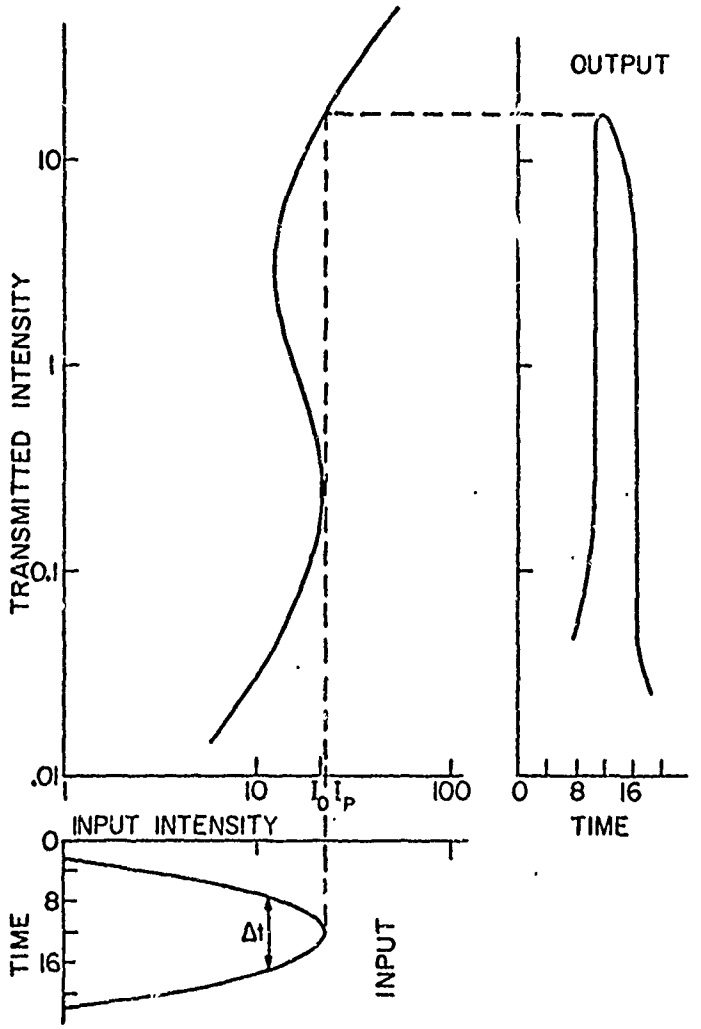

Figure II.C.6. Pulse shaping for a saturable resonator operating in the bistable region.

asymmetry about the peak. This is due to the hysteresis of the saturable resonator when it operates in the bistable region. With the proper saturable absorber, i.e., one with small residual absorption, the discontinuous jump to the "on" state can be several orders of magnitude.

Figure II.C.7 shows the effect of change the relative values of I_0 and I_p. This can be done either by changing the saturable resonator parameters or changing the intensity of the incident pulse. In either case the pulse shaping will be quite different.

For instance if I_0 is much less than I_p, little pulse narrowing will be seen. The dramatic changes in transmission occur in the wings of the Gaussian and the main part of the pulse operates in the linear region of the upper portion of the transfer curve. Negligible pulse shaping is also the case if I_0 is much greater than I_p, for now the saturable resonator operates on a linear region and the transmitted beam simply appears greatly attenuated. In Figure II.C.7, curve 1 is the case for $I_p << I_0$, curve 2 is the case for $I_p \geq I_0$ and curve 3 is the case for $I_p >> I$. All curves are for an incident pulse with a FWHM of Δt.

Figure II.C.8 shows a similar transfer curve, but for normal operation. Again by picking the relative values of I_0 and I_p it is possible to get a good deal of pulse

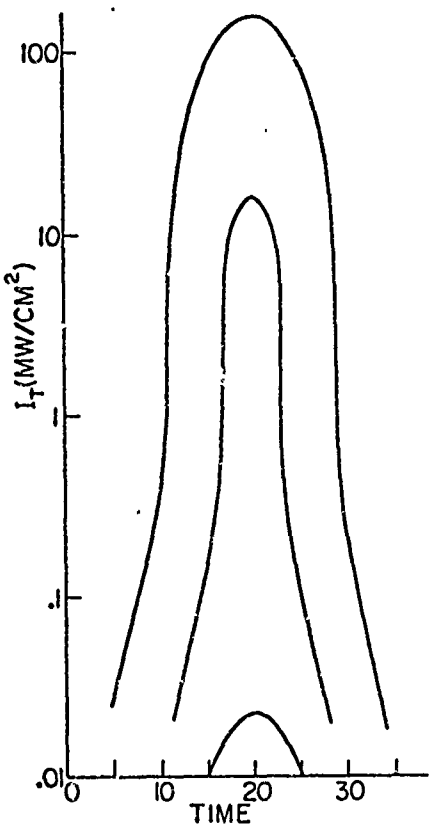

Figure II.C.7. Resultant pulses arising from different relative values of I_0 and I_p.

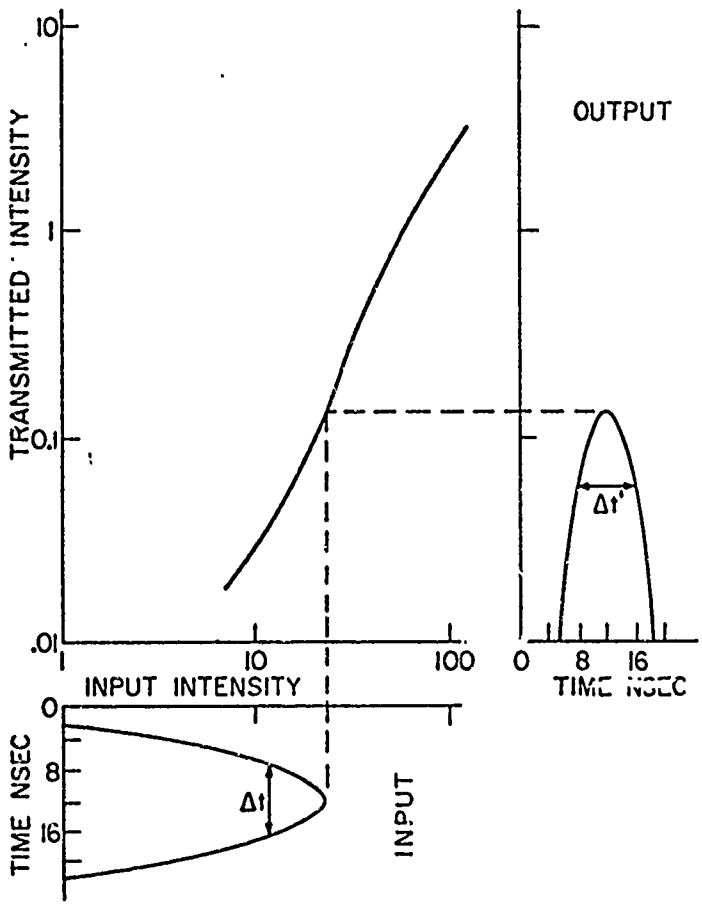

Figure II.C.8. Pulse shaping for a saturable resonator operating in the normal region.

narrowing as seen in the figure. It is seen that for normal operation, however, there is no pulse asymmetry upon transmission. This is the real distinguishing feature of the two types of operation.

III. THE EXPERIMENT

A. The Laser.

The laser used in the experimental work was a giant pulse ruby laser operating in single mode. A beam profile which is nearly Gaussian was obtained by operating with a cavity Fresnel number of approximately 0.5. This type of system and its operation was first described by G.L. McAllister in his doctoral dissertation.[34,35] It was found that even when operating with this cavity configuration, the alignment of the cavity mirrors was very important in determining the time resolved spacial profile of the beam. Small misalignments of the mirrors caused an apparent beam walk-off, with the pulse starting to build up toward one edge of the cavity aperture and progressing to the other edge. Appendix A gives further details on these effects and the method of dynamic alignment used to eliminate this problem.

Figure III.A.1 shows the configuration of the laser cavity. The laser rod was a 3 inch by 1/4 inch ruby rod grown by Union Carbide Corporation. The rod ends were polished flat and parallel and antireflection coated with a hard coating of MgF_2 by Herron Optics. The radial surface was roughened so that it appeared diffuse. The rod temperature was monitored with a thermocouple held in

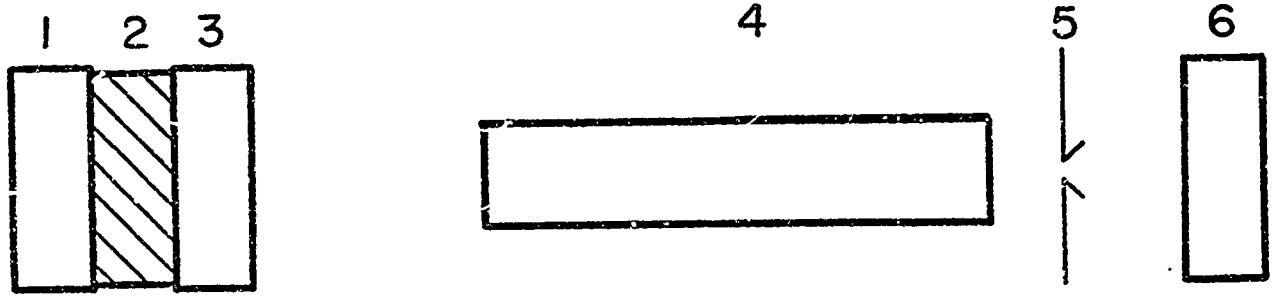

Figure III.A.1. The ruby laser. (1) 99% reflector. (2) Q-switch dye. (3) Window. (4) Ruby rod. (5) Aperture. (6) Output etalon.

contact with one end of the rod. The rod was held in a glass tubing jacket and the whole assembly was mounted in a gimballed support.

The flash tube cavity was a machined single ellipse with the ruby at one focus of the ellipse, but not in mechanical contact with the cavity. The linear flash tube (E.G.&G. FX-45A) was located at the other focus, and the entire flash tube cavity was cooled by the boil-off of liquid nitrogen in a dewar. The flash lamp cavity was mounted in such a way that it was mechanically isolated from the optical bench. Care was taken to keep the cold N_2 from passing through the optical path of the laser cavity.

The back reflector was an optical flat with a highly reflecting dielectric coating (99%+) supplied by Perkin Elmer. Damage threshold was quoted to be greater than 300 MW/cm^2. The output reflector was a Perkin Elmer general purpose window which operated as an etalon giving a maximum reflection of 15%. It was mounted in a Lansing differential screw Angular Orientation device.

The passive Q-switch was a solution of cryptocyanine in methanol which was contained in a spacer between a general purpose window and the back reflector. The spacer was a stainless steel ring with O-ring grooves on the end surfaces. The O-rings were made of ethylene

propylene rubber which could be used with a variety of organic solvents.

The passive Q-switch and etalon, coupled with operating only slightly above threshold, allowed for selection of a single longitudinal mode. Transverse mode selection was obtained by putting a small aperture in the laser cavity.

The output of the laser was nearly Gaussian in time with a typical full width at half maximum of 15 nsec. The radial profile at a particular point in the far field of the cavity aperture was measured by scanning the beam with a small pinhole. Appendix B gives the instrument broadening of the beam width due to this type of pinhole measurement. The pinhole was attached to a Line Tool Company x,y Translator allowing positioning to within .0005 inches. Under optimum conditions of alignment, the output intensity is on the order of 70 MW/cm^2 and with slight misalignment this could be increased by a factor of 2 or more. This misalignment, however, was undesirable since it caused a distortion to the output beam, making it difficult to determine output intensities.

B. Search for Proper Saturable Absorber.

1. Experimental Set-Up

To find a saturable absorber which would meet the criteria for bistable operation, it was necessary to determine the saturated absorption behavior of any of the possible candidates. Huff and DeShazer[12] had parameterized cryptocyanine dissolved in methanol and it was determined from these parameters, and the theory developed for the saturable resonator, that bistable operation would not be possible. It was then decided that dissolving cryptocyanine in other solvents might lower the residual absorption. Measurements using the Cary 14 spectrophotometer indicated that the different solvents did indeed change the wavelength of the absorption peaks a small amount, however, the optimum positioning seemed to be for the methanol system. There was also evidence that the viscosity of the solvents as well as impurities affect transition rates. It had been shown by Huff and DeShazer[12] that cryptocyanine was a steady state system for laser pulse widths on the scale of 10 nsec. or greater. Another organic dye related to cryptocyanine[36] had been used as a passive Q-switch for ruby lasers. This dye, 1,1'-diethyl-2,2'-dicarbocyanine iodide or DDI, displayed a larger degree of mode locking than had cryptocyanine, indicating it perhaps had a shorter time constant and smaller residual absorption. Reports had

also shown that solvents other than methanol worked better in passive Q-switches for mode locking. Specifically, these solvents were acetone and acetonitrile and since their viscosities were almost half that of methanol, it was decided to try these two solvents. A semiconductor glass saturable absorber composed of Cd:Se:S mixed in glass was obtained from Litton Industries. The Cary 14 spectrophotometer indicated the band gap was near 6943Å with transmission of about 36% at 6943Å (excluding surface reflection).

Figure III.B.1 shows the experimental configuration used in the transmission saturation studies. The incident intensity was varied by changing the transmission of the $CuSO_4$ solution in the attenuation cell. A beam-splitter diverted a small portion of the beam before it went into the transmission experiment. This was then sent into an R.C.A. 7102 photomultiplier with an S-1 surface. The photomultiplier was wired as a photodiode and the output was integrated with an R C integrating circuit and was recorded on a Tektronix model 555 oscilloscope with a Tektronix type 1A1 plug-in unit. The voltage output was then prcportional to the energy in the laser pulse. Actually the integration was done by charging the capacitor and the output voltage is across this capacitor. It would be more correct, therefore, to say the energy in the laser pulse is proportional to the square of the voltage, but

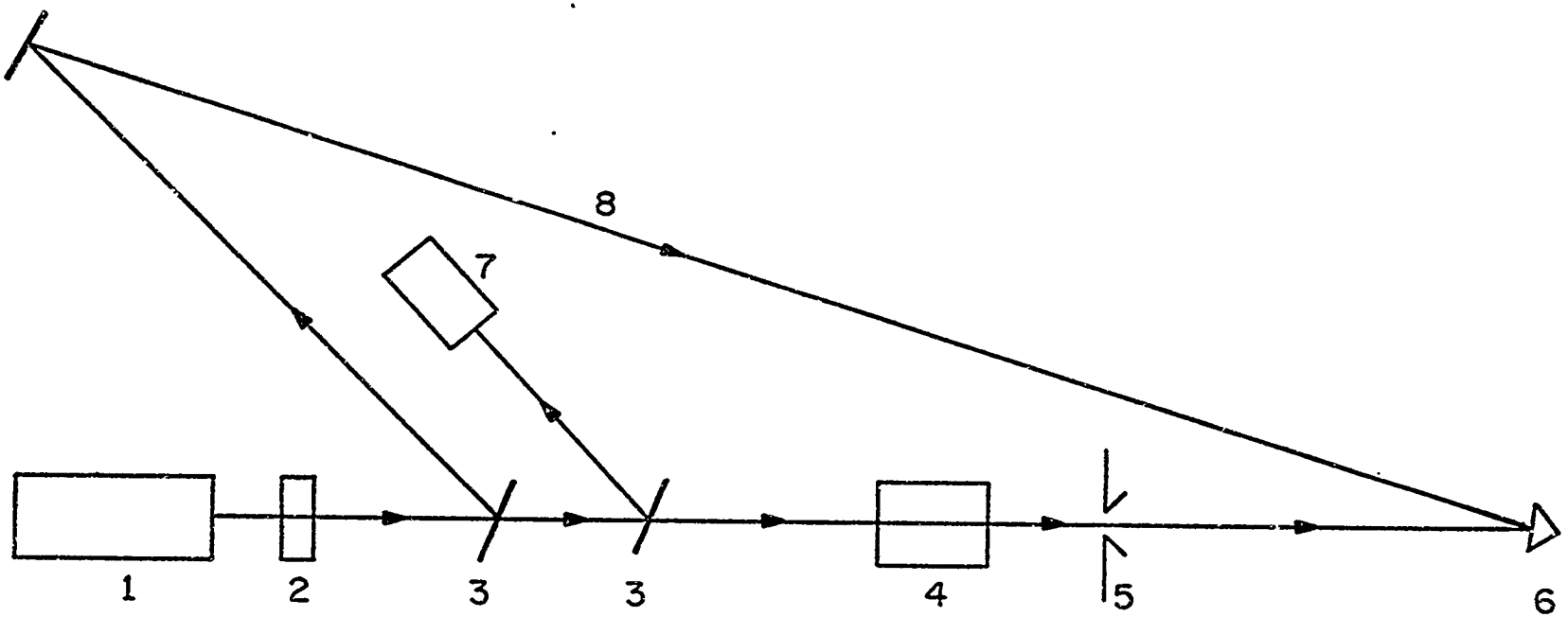

Figure III.B.1. Experimental configuration. (1) Ruby laser. (2) Attenuator. (3) Beam splitter. (4) Saturable absorber cell. (5) Pinhole aperture. (6) ITT photodiode. (7) RCA 7102 photomultiplier. (8) Optical delay line.

with the use of attenuators, the system was operated in a range of the E vs V curve such that the slope was linear to a good approximation. A TRG Model 100 Ballistic Thermopile was then used to calibrate this system. Another beam-splitter deflected a small part of the beam into an optical delay line. The delay line was 45 nsec. in length and was calibrated to give the input power into the transmission cell. By measuring the beam profile it was then possible to determine the intensity. A pinhole was mounted behind the transmission cell and was positioned such that it was centered on the beam and only transmitted a small portion of the center of the beam. The part of the beam then measured was almost constant if the pinhole diameter was much less than the full width at half maximum of radial profile of the beam (see Appendix B).

The beam passing the pinhole and the beam from the delay line both went to the same detector. This detector was an ITT F4000 photodiode with an S-1 surface. The output was recorded on a Tektronix 519 traveling wave oscilloscope. The estimated risetime of the system was .4 nsec and had a fixed gain. The fixed gain made it necessary to attenuate the two beams with neutral density filters as the $CuSO_4$ concentration was varied. The transmission of these filters were measured on a Beckman DK-2 spectrophotometer. For the organic dye saturable absorbers the

transmission of the cell was checked with the particular solvent to be used. This loss could then be corrected for when the transmission of the dye in the solvent was measured. A similar technique was used to measure the transmission of the semiconductor glass but here the surface loss was assumed to be from the Fresnel reflection of the glass. This reflection could then be obtained from the index of refraction of the glass. Steady state type response of the saturable absorbers was checked by comparing the transmitted and delayed pulse shapes. This was done by making a one to one correlation of the increasing and decreasing edges of the transmitted pulse to the delayed reference.

2. Results

a. 1, 1'-Diethyl-2, 2'-Dicarbocyanine Iodide in Methanol.

The results of the transmission measurements of this saturable absorber system are shown in Figure III.B.2. The points indicate the experimental data. The unsaturated transmission of the solution was 31%. A least squares polynomial fit was used to obtain a best fit of the data. The dashed curve indicates the results of this fit using a third degree polynomial. The standard deviation of the curve is .11 and the standard error of estimate for T is .042. The solid curve represents the theoretical results of

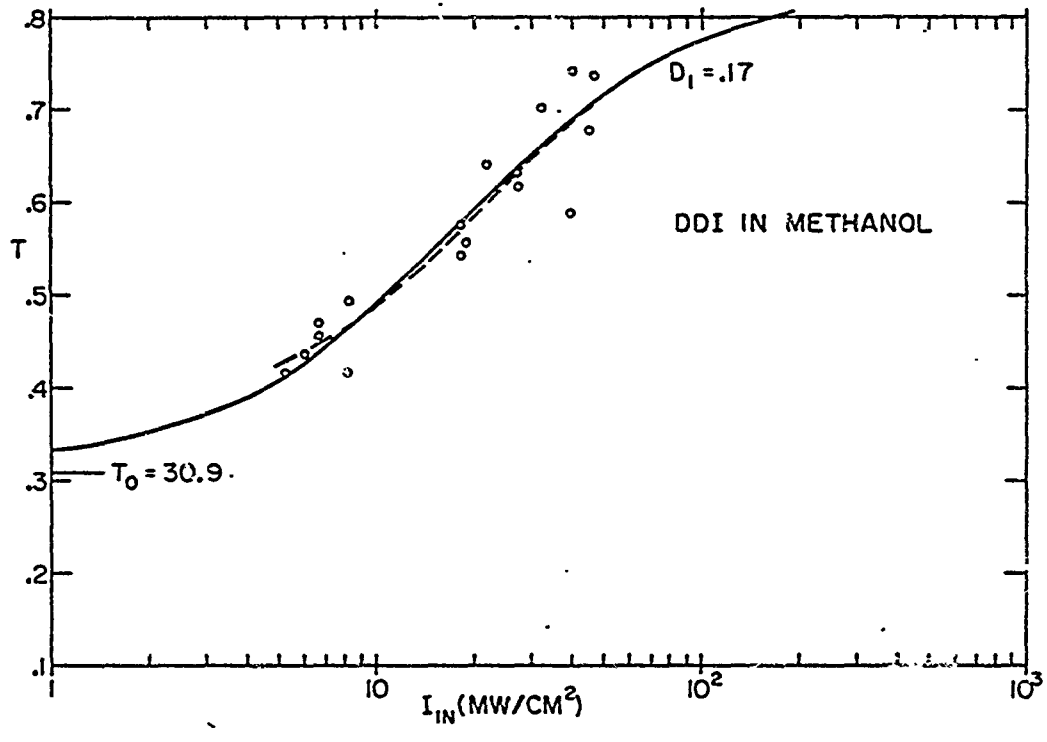

Figure III.B.2. DDI dissolved in methanol. Circles are the experimental data points and the solid curve represents theory.

Section II.B (see equation 1, II.B.10). The parameters for this curve are $D_1 = .167^{+.09}_{-.04}$ and $D_2 = 59.2$.

b. 1, 1'-Diethyl-2, 2'-Dicarbocyanine Iodide in Acetonitrile.

Figure III.B.3 shows the results of the transmission studies for this solution. The low level transmission in this case was 16%. Again a least squares fit with a third degree polynomial was done (dashed curve). In this case the standard deviation of the curve is .10 with a standard error of estimate for T of .035. The solid curve is the theoretical fit from equation 1 of Section II.B.10 using values for the parameters D_1 and D_2 of $.125^{+.04}_{-.01}$ and 171, respectively.

c. 1, 1'-Diethyl-2, 2'-Dicarbocyanine Iodide in Acetone.

Here the unsaturated transmission was 19%. The results are shown in Figure III.B.4 as before. The least squares fit was done with a second degree polynomial. The curve has a standard deviation of .16 and the standard error of estimate for T is .047. The parameters for the theoretical curve are $D_1 = .11^{+.03}_{-.01}$ and $D_2 = 95$.

d. Cryptocyanine in Acetonitrile.

Figure III.B.5 shows the results for a solution with unsaturated transmission of 16%. The dashed curve

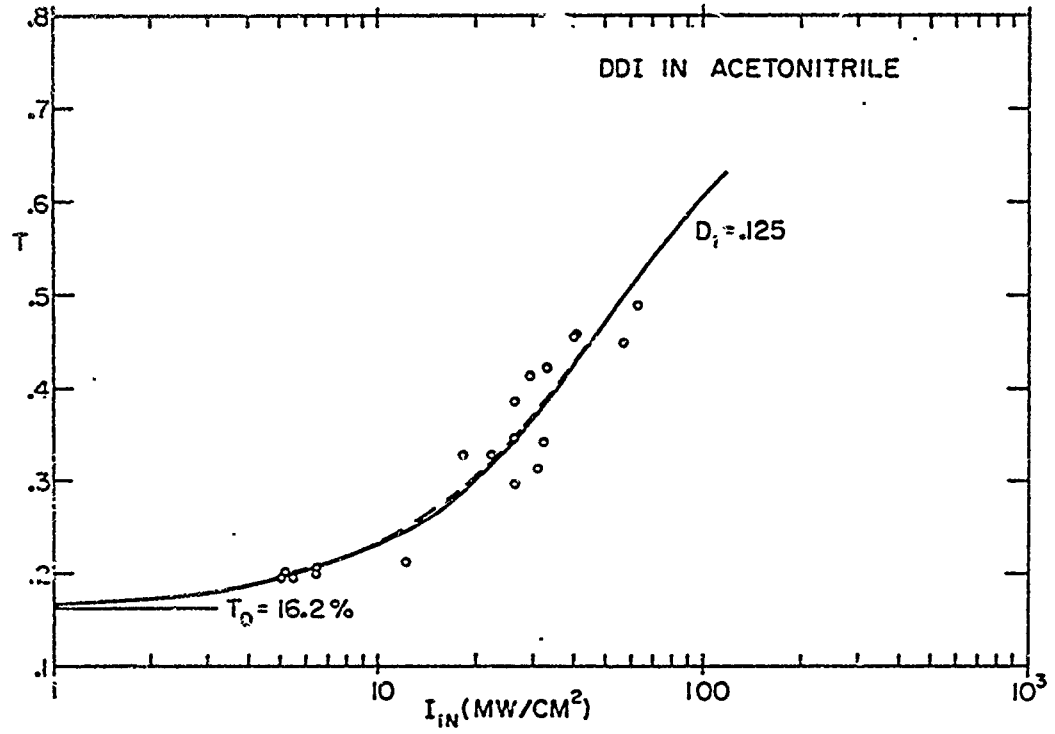

Figure III.B.3. DDI dissolved in acetonitrile. Circles are the experimental data points and the solid curve represents theory.

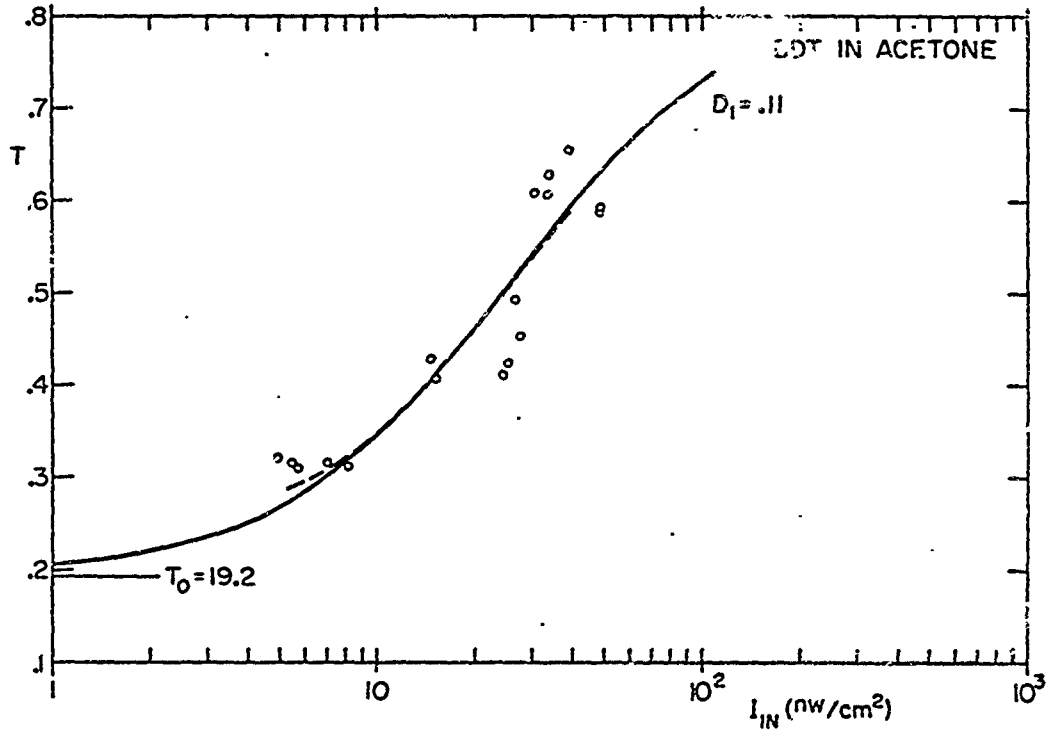

Figure III.B.4. DDI dissolved in acetone. Circles are the experimental data points and the solid curve represents theory.

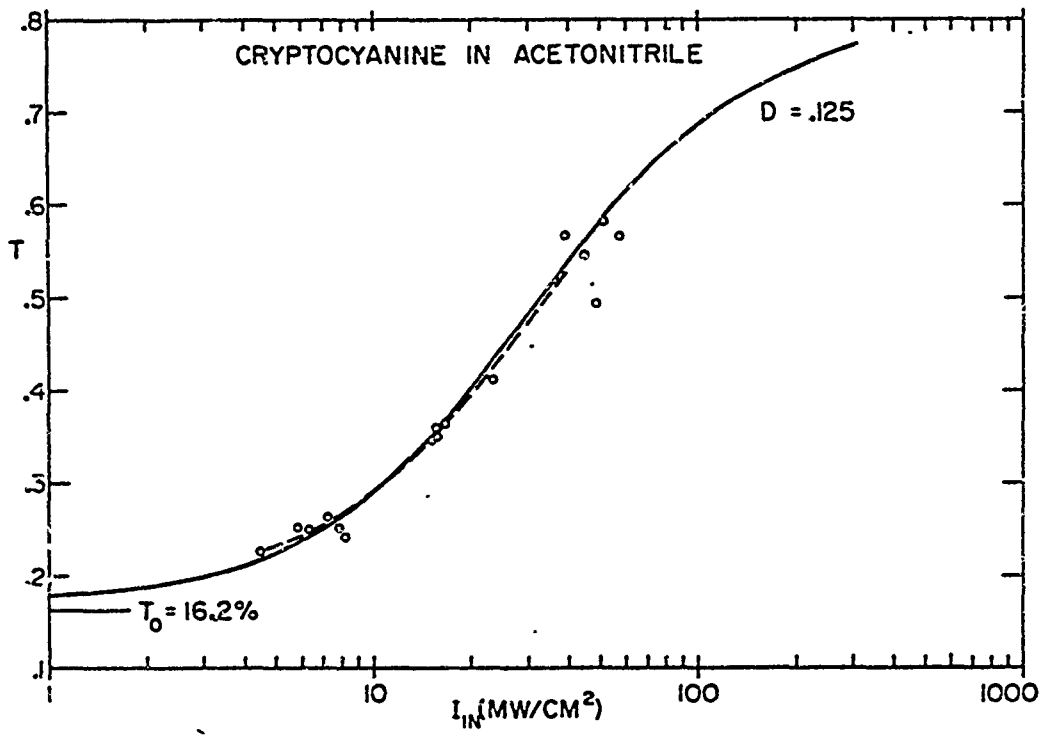

Figure III.B.5. Cryptocyanine dissolved in acetonitrile. Circles are the experimental data points and the solid curve represents theory.

illustrates a third degree polynomial fit to the data. This curve has a standard deviation of .13 with a standard error of estimate for T of .024. The parameters for the solid curve (theoretical) are $D_1 = .125^{+.04}_{-.01}$ and $D_2 = 83.7$.

e. Cryptocyanine in Acetone.

The results of this study are illustrated in Figure III.B.6. The unsaturated transmission was 16%. Again the data was fit with a third degree polynomial which is indicated by the dashed curve. The standard error of the estimate for T was .054 and the standard deviation was .13. The theoretical curve was fit with values for the parameters of $D_1 = .167^{+.09}_{-.04}$ and $D_2 = 70$.

f. Semiconductor Glass Saturable Absorber.

Figure III.B.7 shows the results of the transmission study for the semiconductor glass. Initial transmission for this sample was 36%. The points indicate experimental data which was corrected for surface reflection. The solid curve is the theoretical curve with parameters $D_1 = .083$ and $D_2 = 5.0$. It can be seen in this measurement that the laser intensity was great enough to saturate the absorber completely. The residual absorption was then directly measurable and the above value of D_1 was obtained.

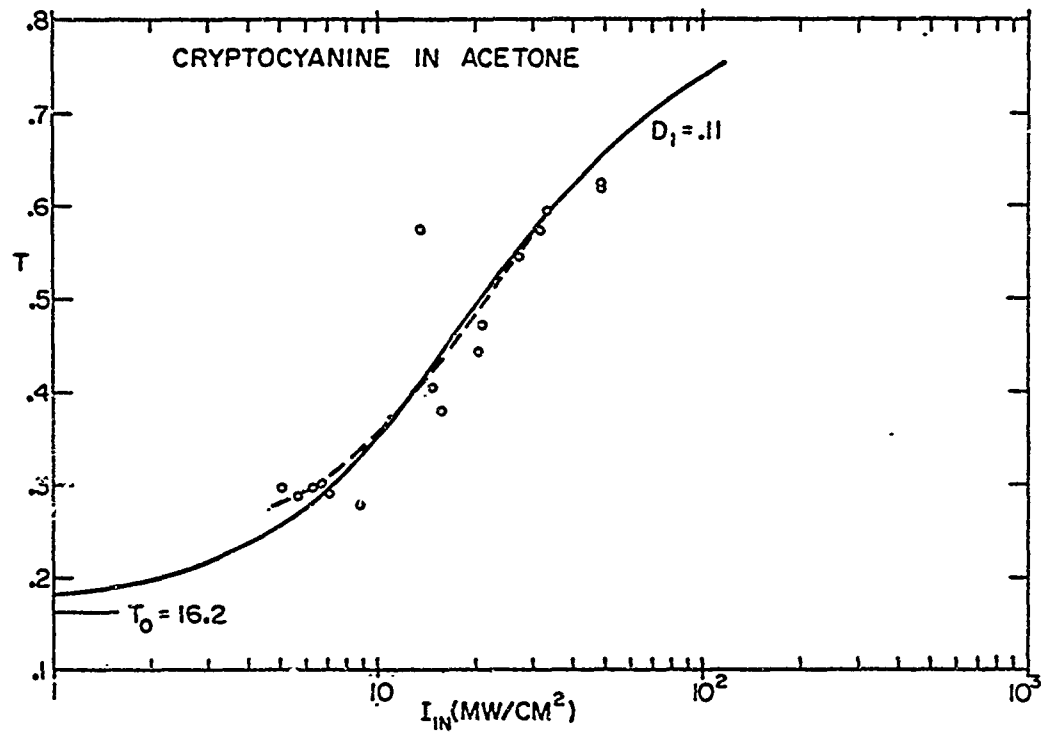

Figure III.B.6. Cryptocyanine dissolved in acetone. Circles are the experimental data points and the solid curve represents theory.

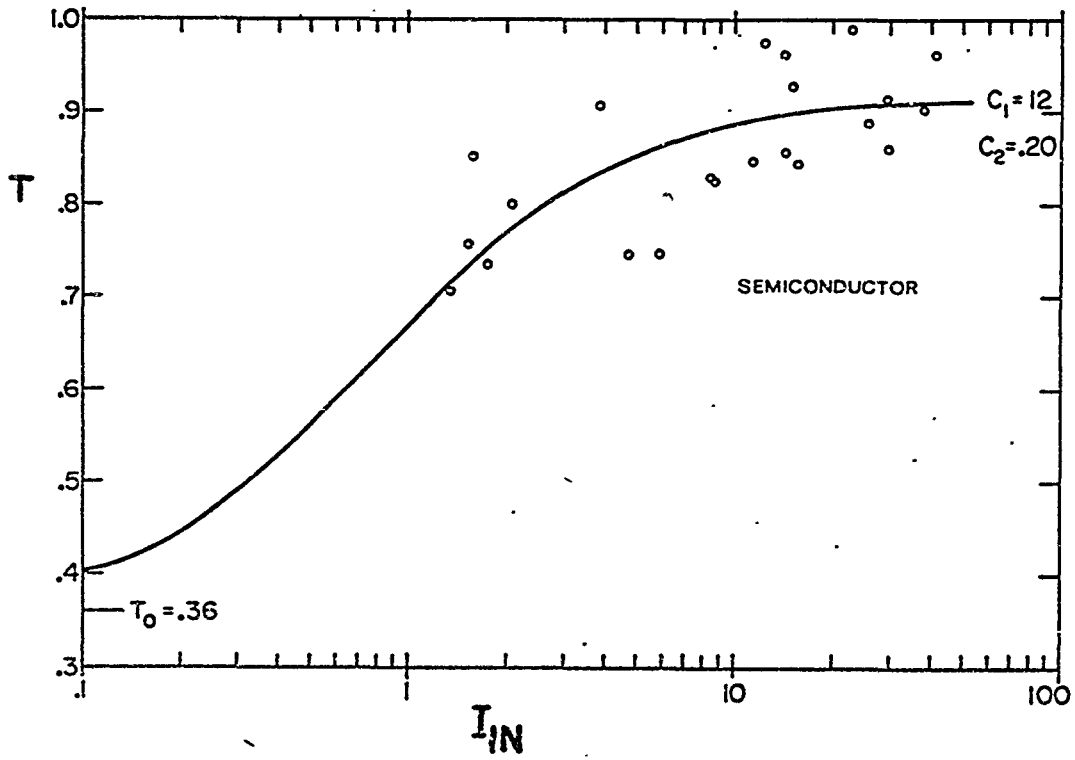

Figure III.B.7. Semiconductor saturable absorber. Circles are the experimental data points and the solid curve represents theory.

C. The Saturable Resonator Using Cryptocyanine in Methanol.

1. Experimental Set-Up

The first attempt to operate the saturable resonator was made using the parameters discussed in the paper by Szöke et. al.[2] In this case cryptocyanine in methanol was fitted with a single absorption model, thus neglecting residual absorption. From here it was easy to get the values for absorber transmission and mirror reflectance parameterized in reference (2) for bistable operation. Three sets of mirrors were used in this phase of the experiment. With each pair the initial transmission of the cryptocyanine in methanol had to be different in order to operate in Szöke's bistable region. The mirror reflectivities used were 99+%, 92.5% and 80% with ranges of initial transmissions of 70 to 80%, 20 to 30%, and 2 to 10%, respectively. The transmission could be adjusted so that approximately the same input intensity should give both states of bistable operation for any of these three sets of mirrors according to Szöke's results.

Figure III.C.1 shows the construction of the saturable resonator used in this part of the experiment. The cryptocyanine was contained inside a spacer between a general purpose window and the input mirror. The mirror was mounted in a Lansing Angular Orientation Device, and

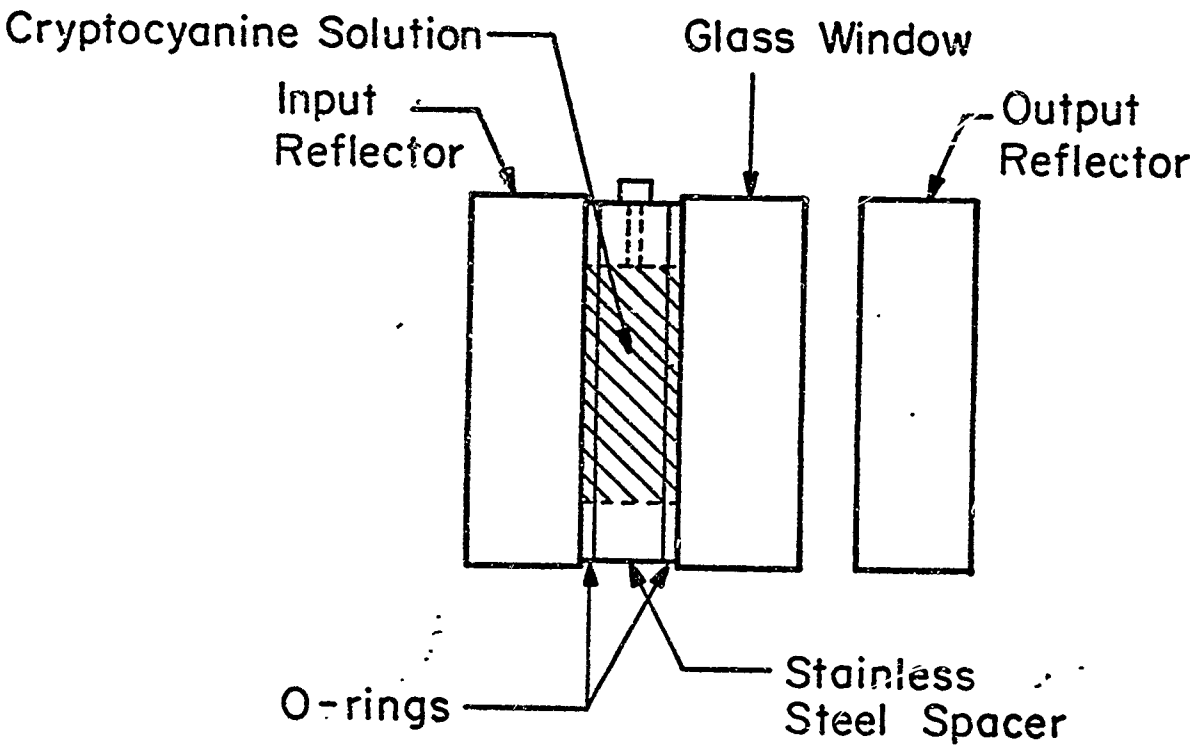

Figure III.C.1. Saturable resonator construction for experiment with organic dye solutions.

this in turn was mounted on a triangular Ealing optical bench. The spacer was constructed of stainless steel with O-ring grooves in the surfaces in contact with the windows to prevent leakage. An opening in the spacer permitted filling of the cell or changing of the solution. Pressure was applied to the general purpose window by means of a retainer ring and three screws. This compressed the O-rings and held the spacer in place. Adjustment of the pressure distribution of the screws permitted alignment of the window with the input mirror to reduce cavity loss. The output mirror was also mounted in a Lansing Angular Orientation Device and put on the same Ealing bench. Mirror separation varied between 2 and 3 cm.

Figure III.C.2 depicts the experimental set-up used to measure the characteristics of the saturable resonator. The system was essentially the same as for the saturable absorber transmission studies except for the addition of a polarizer and quarter wave plate. The polarizer was oriented parallel to the polarization of the laser output and the axes of the quarter wave plate were at 45° with respect to the polarizer. The quarter wave plate was actually a variable wave plate Babinet-Soleil Compensator purchased from Karl Lambrecht. The system of polarizer and quarter wave plate acted to optically isolate the saturable resonator from the laser cavity.

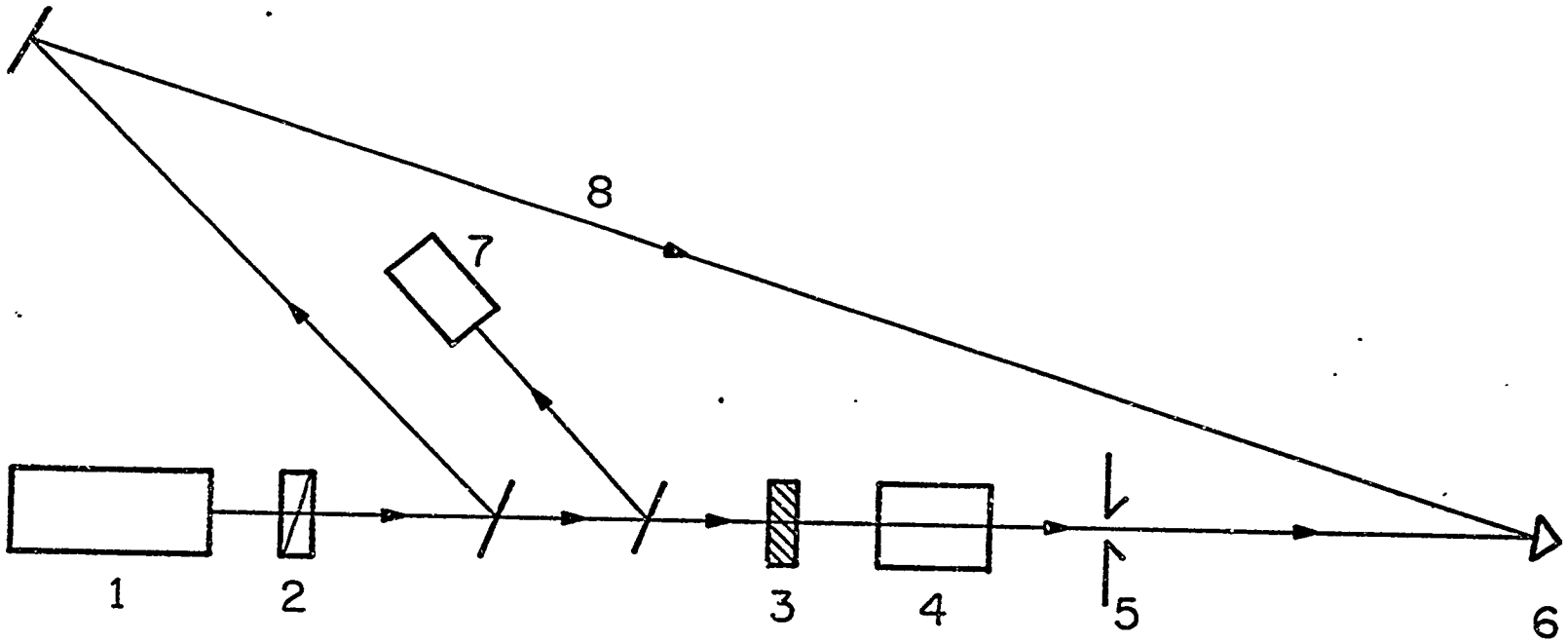

Figure III.C.2. Experimental configuration for saturable resonator. (1) Q-switched ruby laser. (2) Polarizer. (3) Quarter wave plate. (4) Saturable resonator. (5) Pinhole aperture. (6) ITT photodiode. (7) RCA 7102 photomultiplier. (8) Optical delay line.

This caused interference with the laser and destroyed the pulse form but this is prevented by using the isolator. The isolator alignment is described in Appendix C.

The interferometer system was aligned by first orienting the input mirror normal to the laser beam with a He-Ne alignment laser. The output reflector was then aligned parallel to the input mirror by optimizing the circular Fabry-Perot rings. The source used to produce the rings was a He-Ne laser beam passed through a ground glass diffuser and viewed with a telescope.

2. Results

Three different interferometer cavities were used in this part of the experiment. Each had different mirror reflectivities and different low level absorber transmissions. The first had mirror reflectivity of R=99+% and absorber transmission T_0=85%. In this case mode matching difficulties and cavity characteristics caused transmission of the resonator to be such that the nonlinear region was not detectable. There was no pulse shaping in this case.

The other two cavities (R=92%, T_0=23% and R=80%, T_0=8%) gave pulse shaping and suitable transmission for measurement. Pulse narrowing was obtained and in some cases this approached 50% but no bistable operation with resulting hysteresis was observed. At first this was

attributed to the problem of matching the laser longitudinal mode with the "on-resonance" mode of the saturable resonator but was subsequently attributed to the neglect of residual absorption in Szöke's model. Figures III.C.3 and III.C.4 show plots of the theoretical curves with data points superimposed. The data points for the R = 80% case were taken with no pinhole behind the saturable resonator. In the case of the R = 92% mirror data points were taken both with and without a pinhole.

The different intensity levels were obtained by measuring corresponding points on the oscilloscope trace of the incident and transmitted pulses. Care was taken that the time variation of the pulse was the same over the entire spatial profile of the beam. Comparing the peak intensities of each pulse shows the maximum transmission obtained of the saturable resonator was .92% for the R = 92% case and 2.9% for the 80% case.

Figure III.C.5 shows the example of pulse narrowing obtained in certain cases. The pulse on the right is the time evolution of the incident intensity, while the pulse on the left is the time evolution of the same pulse after passing through the saturable resonator. Figure III.C.6 illustrates several conditions showing the effects of the different components of the saturable resonator.

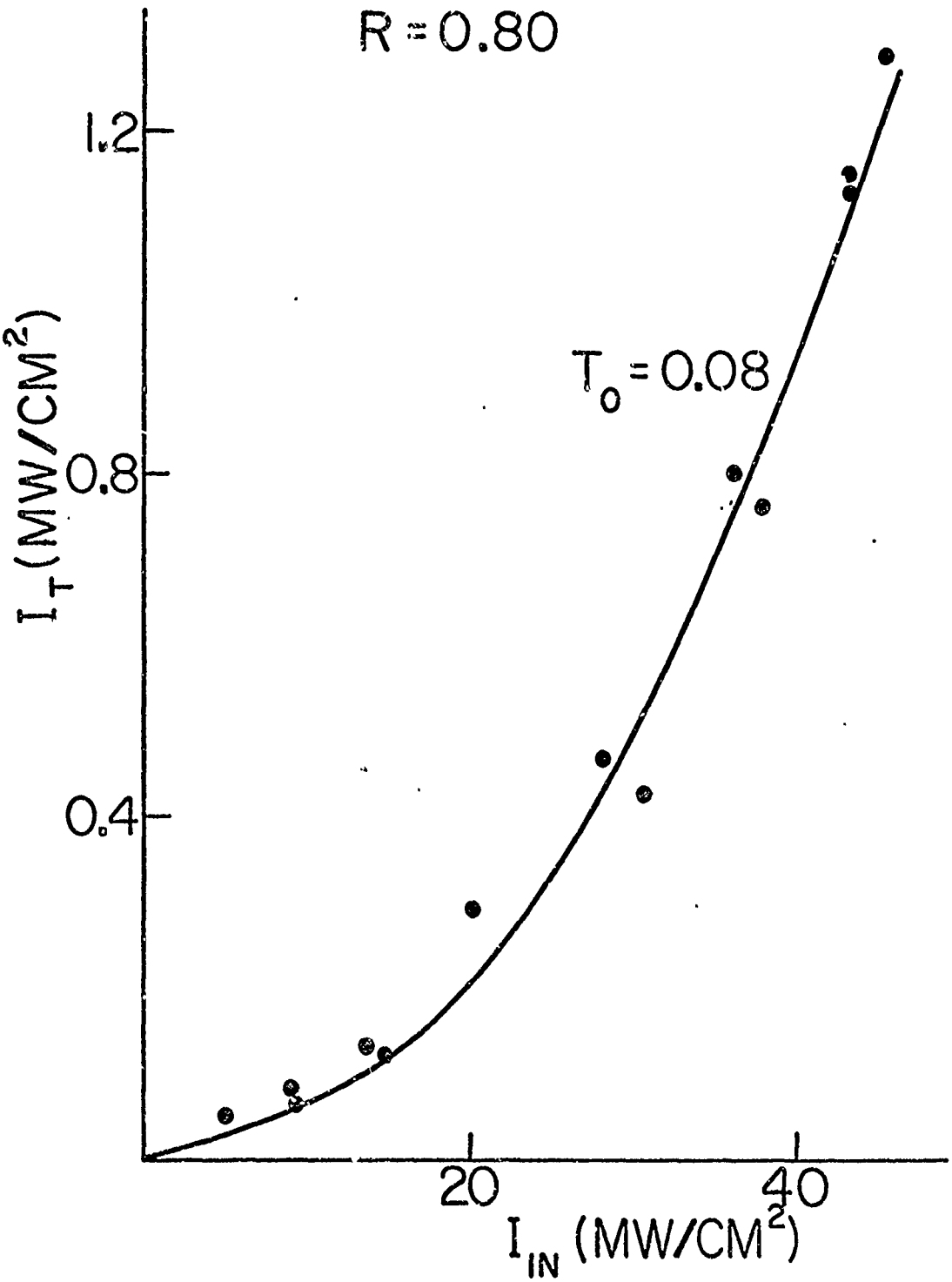

Figure III.C.3. Experimental data points and theoretical curve for saturable resonator containing cryptocyanine in methanol.

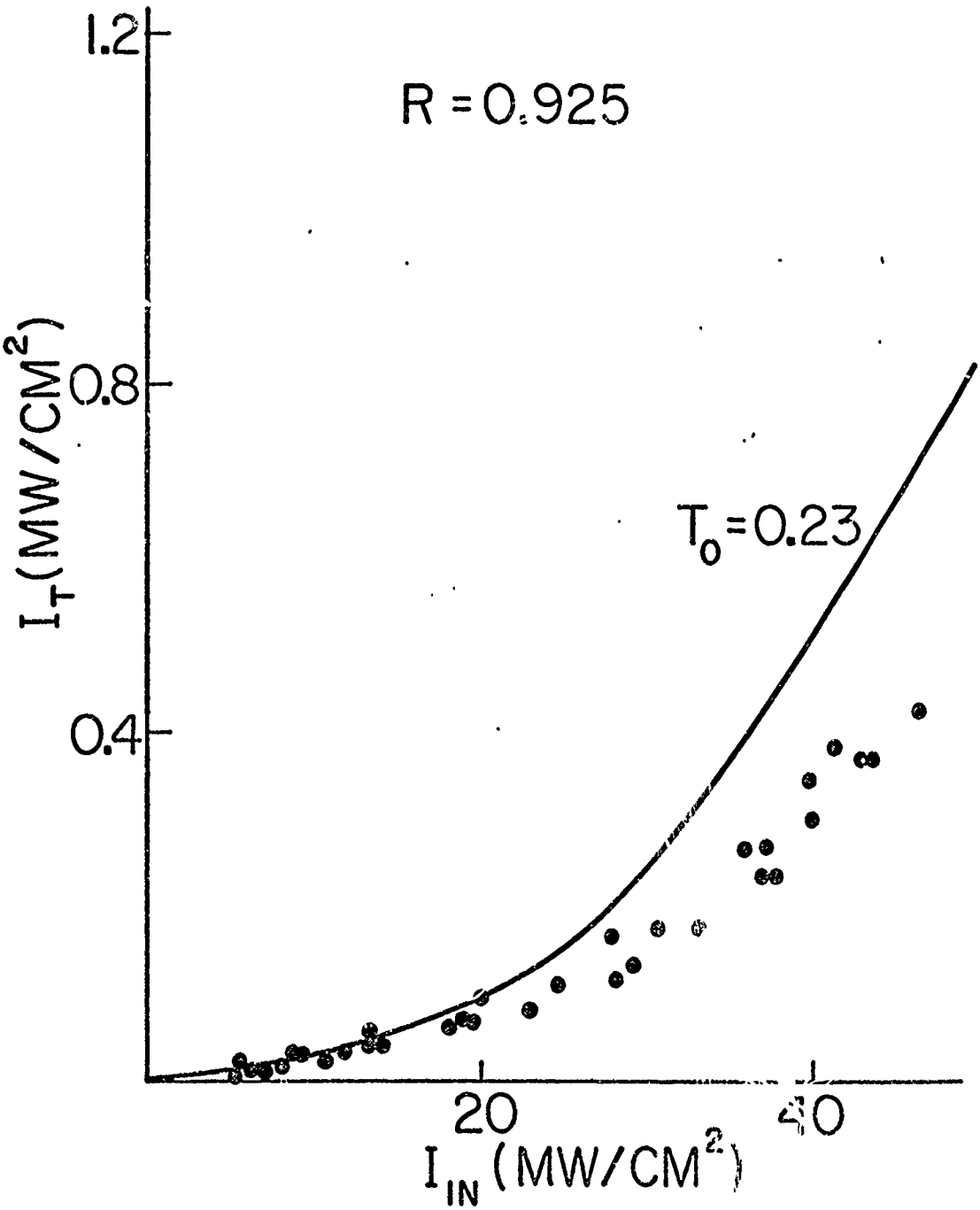

Figure III.C.4. Experimental data points and theoretical curve for saturable resonator containing cryptocyanine in methanol.

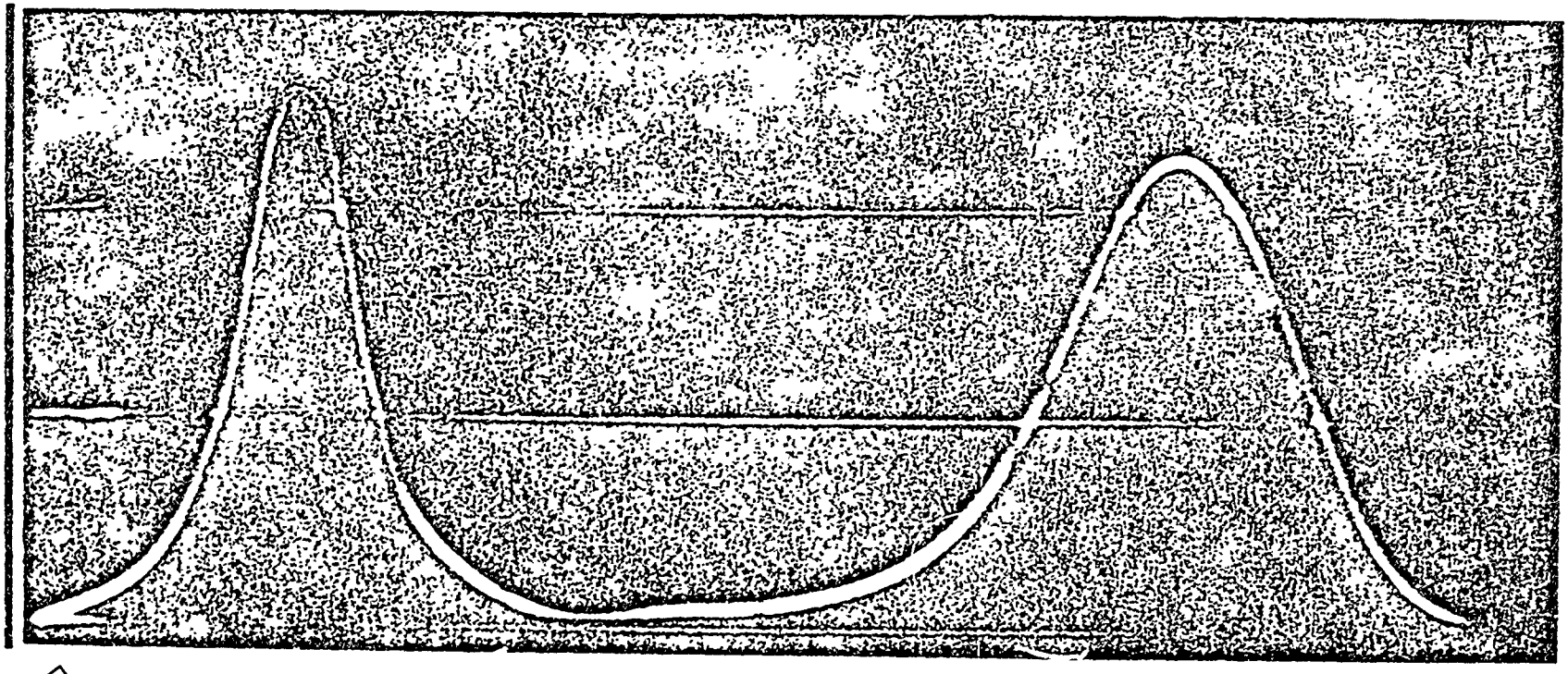

Figure III.C.5. Pulse narrowing from the saturable resonator.

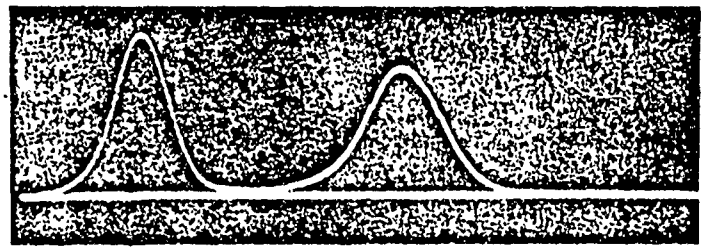

(a) Dye only T_0 = 8%.

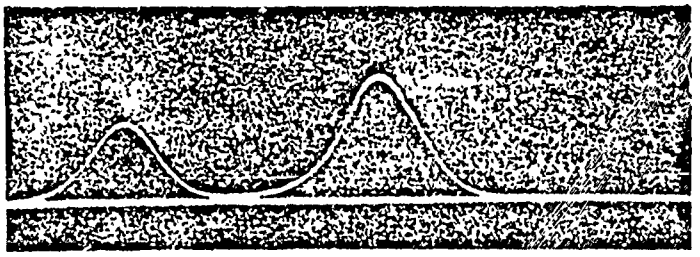

(b) One reflector only.

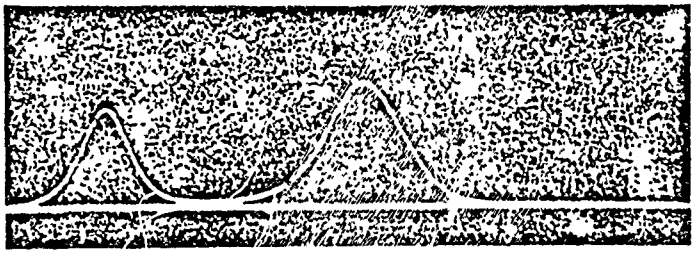

(c) Resonator containing saturable dye.

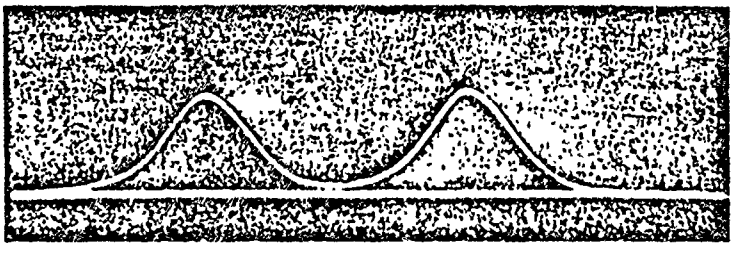

(d) Resonator without dye.

Figure III.C.6. Effects of several components of the saturable resonator.

D. Saturable Resonator with Absorber Meeting Bistable Criteria.

1. Experimental Set-Up

The transmission experiment indicated several saturable absorber systems had the potential for bistable operation. The organic dye/solvent systems which met the criteria were again used in the arrangement as shown in Figure III.C.1. The pairs of mirrors available for the work had individual reflectivities of 99+%, 92.5% and 80%. There were several other single mirrors with reflectivities of 97% and 95%. This, along with the maximum laser intensity and absorber parameters, determined which mirrors could be used and the range of unsaturated transmission, T_0, which would work.

The semiconductor glass saturable absorber transmission studies showed that this saturable absorber would meet the criteria for bistable operation. However, for this case, the unsaturated transmission T_0 was not variable thus restricting the range of mirror reflectivities. Available laser output intensities and limitations on smallest detectable saturable resonator output intensities further restricted the mirror reflectivities that could be used. The system was tested in two ways for the semiconductor case. First the resonator cavity was constructed of two external mirrors and the absorber suspended between

them. The minimum mirror separation was 3 cm. This failing to work, it was then decided to coat one surface of the absorber for high reflection and align it to an external mirror. This would remove one source of surface loss in the cavity. The other side of the absorber was antireflection coated, thus reducing loss from that surface. Minimum mirror separation in this case was about 3 mm, the limitation being the thickness of the absorber. The coated semiconductor glass was also mounted on a piezoelectric drive in an attempt to try to match modes of the laser.

Since the semiconductor band gap fell at 6943Å, the transmission was very low for wavelengths less than this. This caused great difficulty in aligning the resonator cavity since the only source available to do the alignment was a 6328Å He-Ne laser. Fabry-Perot interference rings were faintly visible in a dark room with some difficulty, but optimizing them was almost impossible.

The configuration used to measure the characteristics of the saturable resonator for the above cases is essentially the same as described in Section III.C. A diagram of the experiment is given in Figure III.C.2.

2. Results

a. Organic dyes.

The transmission studies of the dye solutions in-

dicated that 1, 1'-diethyl-2, 2'-dicarbocyanine iodide or cryptocyanine dissolved in acetone could best operate the saturable resonator in the bistable regime. However, this bistable operation is limited to a small range of reflectivities ($R \geq .995$) because of the high value of the absorber parameter D_1. The transmission at which there is a change of bistable states was on the order of .05%. This value however depends critically on the mirror reflectivity and the low level absorber transmittance. These low levels of transmission made detection of the hysteresis difficult since this was on the order of the minimum transmitted intensity detectable at peak laser intensities. Intensity levels necessary to drive the resonator into the upper transmitting state have a minimum of 45 MW/cm^2, however, errors in determining absorber parameters and mirror reflectivity could greatly change this value. Transmission at this intensity would be on the order of 0.1%. For a typical peak laser output (15 MW/cm) the theoretical transmission was .017%, and this, too, depended on mirror reflectivity and the saturable absorber parameters.

For cryptocyanine in acetone the unsaturated transmission for the case of R = 99+% mirrors was $T_0 = 65\%$. Many shots were taken, however there was only slight transmission and no pulse shaping was seen. Maximum transmission was .03% for an input intensity of 16.3 MW/cm^2. Since

the transmission was so small no pinhole was used. A second case was run for mirror reflectivity of R = 92.5% and unsaturated absorption of 10% for the cryptocyanine solution. The theoretical peak transmission was .1% for the intensities used and the peak transmission measured was .3 to .4%. No pulse shaping was seen.

The experiment was repeated for DDI in acetone with R = 99+% mirrors and unsaturated absorption of 68%. Maximum observed transmission was again on the order of .05% with no noticeable pulse shaping. However, the maximum transmitted pulse was barely detectable. DDI was also run with mirror reflectivity of 92.5% and low level absorber transmission of 10%. Again peak intensities were in the range of .3% with a .1% theoretical transmission.

b. Semiconductor Saturable Absorber.

For the semiconductor saturable absorber in the saturable resonator several configurations were used. First the absorber was placed between two mirrors each with reflectivity of 99+%. In this case there was no measurable transmission after many shots. Peak input intensities were on the order of 20 MW/cm^2. The theoretical intensities needed to drive the saturable resonator into the higher transmission state was 7.6 MW/cm^2. Peak theoretical transmission should have been .6%.

In order to try to increase the transmission, the mirror reflectivity was reduced to R = 92.5%. In this case no pulse shaping was observed. Peak input intensities were in the range of 15 to 20 MW/cm^2 with peak transmission of 3.8%. No pulse shaping was seen and, theoretically, for these saturable resonator parameters, the system should not be in the bistable region.

Next, one surface of the semiconductor was reflection coated for a reflectivity of 99%. It was mounted on a piezoelectric ceramic to vary mirror separation to try to match to the longitudinal modes of the laser cavity. As expected, the laser was never operating on the same mode from shot to shot, so again there was no measurable transmission.

IV. CONCLUSIONS

A. Theory.

The theory for steady state operation of a saturable absorber was developed starting with the treatment of a Fabry-Perot interferometer with nonsaturable loss. Resonance characteristics of the interferometer were obtained in terms of mirror reflectivity and cavity loss. With this result it was then possible to replace the unsaturable loss with a saturable loss. In order to do this it was necessary to first develop models for the saturable absorbers used.

A model with excited state absorption previously developed by Huff and DeShazer[12] was extended to include both excited singlet and triplet level absorption. It was then shown that the excited singlet level absorption could be neglected in certain instances. This excited state absorption was responsible for the residual absorption, which was characteristic of the organic dyes used in this work. Methods of reducing the residual absorption were discussed. These methods included using solvents of different refractive indices as well as using solvents of different viscosities. Varying the refractive index shifts the absorption lines and varying the viscosity alters the collision rates with impurities.

A second model, which was applicable to the semiconductor saturable absorber, was also developed. This model involved a single absorption (i.e., valence band to conduction band transition) with an unsaturable loss such as scattering. It was shown that this model had the same functional dependence between transmittance and incident intensity as did the excited state absorption model.

With a mathematical expression for the saturable absorber, it was possible to solve the saturable resonator problem. With this solution a set of criteria were established for operation of the saturable resonator in a bistable regime. It was determined that the residual absorption of the saturable absorber was the limiting factor in obtaining bistable operation. Other factors determining whether bistable operation occurred were mirror reflectivity and low level absorber transmission.

B. Experimental Verification

By using different solvents it was shown that the residual absorption of a particular organic dye could be altered. Each dye was dissolved in three solvents. These were methanol (refractive index 1.331[37] and viscosity 0.547[37] centipoise), acetonitrile (refractive index 1.346[37] and viscosity .345[37] centipoise), and acetone (refractive index 1.359[37] and viscosity .316[37] centipoise). The results of the transmission studies showed that the smallest residual absorption was for cryptocyanine or DDI dissolved in acetone ($D_1 = .11^{+.03}_{-.01}$ for each). Residual absorption was slightly larger for these dyes in acetonitrile ($D_1 = .125^{+.04}_{-.01}$ for each). The residual absorption was largest with cryptocyanine dissolved in methanol. The larger of the two ($D_1 = .315$ for cryptocyanine[12] and $D_1 = .167^{+.09}_{-.04}$ for DDI).

These results indicate that viscosity changes have the larger effect on the residual absorption for the solvents used in this study. It was also determined that cryptocyanine or DDI dissolved in acetone had values of D_1 which could give bistable operation. The parameter D_1 must be less than .118 for bistable operation so that to the degree of determination of this experiment the two dyes dissolved in acetonitrile might also give bistable

operation. In all cases, however, the bistable criterion for the saturable absorber was just barely met. From the transmission experiment it was demonstrated that it was indeed possible to alter the residual absorption and that triplet state quenching was the dominant way of doing this.

The transmission studies on the semiconductor glass saturable absorber indicated that the D_1 parameter was in the bistable region ($D_1 = .083$). The response of the semiconductor glass indicated that it was operating in the steady state regime since there was no asymmetry in the transmitted pulse. It was also found that the semiconductor glass saturated at much lower intensities than did the two dye systems.

The operation of the saturable resonator was first tested in normal operation using cryptocyanine in methanol. By properly adjusting the cavity parameters, R and T_0, it was possible to obtain pulse sharpening up to 50%. The results of this series of tests indicated that in the region of normal operation, the saturable resonator followed the results theoretically predicted.

Next an attempt was made to operate the saturable resonator in the bistable region. Since the saturable absorber parameter D_1 was so large the ranges of reflectivity and low level transmission were severely restricted. It turned out that for the available mirrors

the laser intensity was not great enough to drive the laser into the upper transmitting state. Using the cryptocyanine in acetone and DDI in acetone, the saturable resonator transmission at the intensity levels available were of the same order as theoretically predicted.

Bistable operation was attempted with the semiconductor glass. Since saturation occurred at lower intensities for this absorber, the laser output should have been sufficient to drive the system into the upper transmission state. No measureable transmission was observed for this test. Operating the system out of the bistable region by reducing the mirror reflectivity gave transmissions smaller than those predicted. This was probably due to mode mismatching between the laser and the saturable resonator. Using a piezoelectric to change the saturable resonator mirror separation did not improve transmission of the resonator.

C. Further Work.

In order to get better operation of the saturable resonator, i.e., higher peak transmission, it is desirable to reduce the residual absorption of the saturable resonator. Triplet state quenching seems to be the way to proceed. Experimental investigation into other paramagnetic systems other than O_2 would be a logical step. It might be possible to find substances which have higher solubility thus giving better coupling to the excited dye molecules. A better way of approaching this problem might be to directly measure the triplet lifetime with a probe laser and a pump laser rather than to measure residual absorption. Of course, in the end, it is the amount of residual absorption that is important.

Some of the saturable resonator work was limited by the lack of sufficient intensity from the ruby laser. It would thus be of interest to try the saturable resonator using cavity parameters in the bistable region with a more intense source (greater than 100 MW/cm^2). At present, the saturable absorbers are borderline on giving bistable operation, so it probably is not worth the effort. However, if a better saturable absorber system is found, this effort should prove fruitful.

In this work the problem of coupling the saturable absorber with the interferometer cavity was solved in steady state with an external driving signal. It would now be useful to put a gain medium inside the cavity thus giving a Q-switched laser system. It would be of interest also to solve this problem for the nonsteady state case also.

APPENDIX A

Laser Alignment

The standard method of aligning ruby laser cavities has been to use an autocollimator to give a superposition of reflected images or to use an alignment laser such as a He-Ne laser to produce interference fringes. It has been found that this method produces a time integrated Gaussian shaped spot, i.e. when measured photographically. However, if certain portions of the beam are time resolved using a small sampling pinhole and fast detector, the time dependence of these portions are not the same as that of the total beam. In fact the peak intensities of certain parts of the beam occur at different relative times. It has also been observed that parts of the beam at times have more than one peak, even though the above mentioned alignment procedure indicated "good" alignment.

These problems, however, can be explained by mirror misalignment. A method of correcting this will be described here. Since there is an extra element in the cavity, i.e., the saturable absorber cell window, it is easier to do the alignment if this window is aligned interferometrically with the rear reflector. The remaining surfaces can then be aligned by either of the two methods described above.

Now a pinhole scan of the output beam can be done comparing the beam transmitted through the pinhole to that which goes through the optical delay line. When the laser mirrors are slightly misaligned along the direction of the scan it will be noticed that the separation of the peak intensities of the transmitted and delayed beams varies. The relative pulse widths also vary. By measuring the separation of the peaks it will be noticed that the separation will consistently increase in a certain direction of scan. This indicates the direction of mirror misalignment and appears to be due to the spatial walk-off of the beam as it is reflecting back and forth in the cavity. By correcting this mirror misalignment this problem consistently disappears and the laser output becomes uniform in time across beam. This is true provided transverse mode distortion has been eliminated by the method described by McAlister et. al.[34,35]

APPENDIX B

Error Arising from Measurement of Gaussian Beam with Finite Size Pinhole

The result of measuring a beam of light by scanning with a finite sized circular aperture will be derived here. This involves doing the following convolution integral

$$g(r,\theta) = \int_0^{\infty} \int_0^{2\pi} f_1(r',\theta') f_2(r-r',\theta-\theta') r' dr' d\theta'$$

where $g(r,\theta)$ is the profile measured by the scanning procedure, $f_2(r,\theta)$ is the spatial profile of the light beam, and $f_1(r,\theta)$ is the profile of the transmission of the aperture. For a circular aperture of radius r_0 centered at $r' = 0$

$$f_1(r',\theta') = \begin{cases} 0 \text{ if } r'>r_0 \\ 1 \text{ if } r'<r_0 \end{cases} .$$

For a Gaussian profile beam centered at r, and width of a_0

$$f_2(r-r',\theta-\theta') = \exp\{-(1/a_0^2)[r^2+r'^2-2rr'\cos(\theta-\theta')]\}$$

Using these definitions and equation 9.1.21 of Abramowitz and Stegun[38]

$$g(r,\theta)=2\pi\exp(-r^2/a_0^2)\int_0^{r_0} r'dr'\exp(-r'^2/a_0^2)J_0(\frac{2ir'r}{a_0^2})$$

Since $J_0(iz) = I_0(z)$, where $J_0(z)$ is a Bessel function of zeroth order and $I_0(z)$ is the modified or hyperbolic Bessel Function, it is possible to evaluate the above integral numerically. This is done using the approximation for the modified Bessel Function by equations 9.8.1 and 9.8.2 in Abramowitz and Stegun[38] and the Extended Simpsons Rule method of numerical integration. Several values of the ratio r_0/a_0 were used. For $r_0/a_0 = 0.1$, the measurement of the full width at half maximum would theoretically be within 1% of the actual value, for $r_0/a_0 = 0.5$, it is within 5%, and for $r_0/a_0 = 1.0$, it is within 20%.

These results were experimentally verified by scanning the output beam of the ruby laser with two different sized pinholes: The radii of the two pinholes were .036 mm and .508 mm. The FWHM measured with the smaller pinhole was .406 mm (radius) while the FWHM measured with the larger pinhole was .533 mm (radius).

Appendix C

Further Description of the Optical Isolator

The optical isolator is an optical system which transmits light when the light is traveling in one direction and does not transmit light when the light is traveling in the opposite direction. The method described here is a passive system and is in fact a circular polarizer. The circular polarizer will transmit light of one circular polarization and reject the other. The circular polarizer can also convert linearly polarized light into circularly polarized light and circularly polarized light into linearly polarized light. Since on reflection the direction of circular polarization is changed to the orthogonal polarization, the reflected beam is always rejected.

The system is composed of a linear polarizer and a quarter wave plate oriented such that the principle axes of the quarter wave plate are at 45° relative to the polarizer. The light passing through the polarizer then strikes the quarter wave plate such that the electric field vector has equal components along each of the principle axes. Due to the thickness of the quarter wave plate, one component is retarded in phase by $\pi/4$ relative to the other yielding circular polarization on transmission. The

direction of the polarization will depend on the relative orientation of the linear polarizer and the optic axis of the quarter wave plate. If the linear polarizer is oriented parallel to the polarization of the laser, it is possible to get total conversion if reflective losses, scattering, etc., are ignored. Unfortunately in most cases these losses can be considerable (10-20%).

The alignment of the system involves first maximizing the transmission through the linear polarizer. The quarter wave plate was a Babinet-Soleil compensator which is actually a variable wave plate adjustable over almost 7 full waves of retardation at 6943Å. Thus the orientation, as well as the physical thickness, required adjustment. The calibration supplied with the Babinet-Soleil compensator gave the amount required to change 1 full wave of retardation at a certain wavelength but not the absolute value of the retardation. This was determined by using several different wavelengths to produce circular polarization. It was determined that .20 mm corresponds to -3/4 λ retardation for λ = 6943Å. Knowing this, it was possible to align the angular orientation of the quarter wave plate relative to the linear polarizer with the cw alignment laser. Next the thickness could be adjusted to the ruby laser output. Then by alternately adjusting the orientation and the thickness, the optical isolator could be optimized.

REFERENCES

1. J.E. Bjorkholm, U.S. Patent No. 3,500,241.
2. A. Szöke, V Daneu, J. Goldhar, and N.A. Kurnit, Appl. Phys. Lett. 15, 376 (1969).
3. P.P. Sorokin, J.J. Luzzi, J.R. Lankard, and G.D. Petit, IBM J. Research and Develop. 8, 182 (1964).
4. B.H. Soffer, J. Appl. Phys. 35, 2551 (1964).
5. P. Kafalas, J.L. Masters, and E.M.E. Murray, J. Appl. Phys. 35, 2349 (1964).
6. G. Bret and F. Gires, Compt. Rend. 258, 4702 (1964).
7. W.G. Wagner and B.A. Lengyel, J. Appl. Phys. 34, 2040 (1963).
8. I. Burak, P.L. Houston, D.G. Sutton, and J.I. Steinfeld, IEEE J. Quant. Elect. QE-7, 73 (1971).
9. A.J. Demaria, D.A. Stetzer, and H. Heynau, Appl. Phys. Letters 8, 174 (1966).
10. O.R. Wood and S.E. Schwarz, Appl. Phys. Letters 12, 263 (1968).
11. A.F. Gibson, M.F. Kimmitt, and C.A. Rosito, Appl. Phys. Letters 18, 546 (1971).
12. L. Huff and L.G. DeShazer, J. Opt. Soc. Amer. 60, 157 (1970).
13. M. Hercher, Appl. Opt. 6, 947 (1967).

14. C.R. Guiliano and L.D. Hess, IEEE J. Quantum Elect. QE-3, 358 (1967).

15. V.P. Oppenheimer, P. Melman, IEEE J. Quantum Elect. QE-7, 426 (1971).

16. M. Hercher, W. Chu, and D.L. Stockman, IEEE J. Quantum Elect. QE-4, 954 (1968).

17. L. Huff and L.G. DeShazer, Appl. Opt. 9, 233 (1970).

18. L. Huff, Dissertation, University of Southern California, 1969 (unpublished).

19. O.R. Wood, P.L. Gordon, and S.E. Schwarz, IEEE J. Quantum Elect. QE-5, 502 (1969).

20. I. Burak, A.V. Nowak, J.I. Steinfeld, and D.G. Sutton, J. Quant. Spectrosc. Radiat. Transfer, 9, 959 (1969).

21. B.B. Snavely and F.P. Schäfer, Physics Letters, 28A, 728 (1969).

22. M. Born and E. Wolf, Principles of Optics (Pergamon Press, New York, 1965).

23. S. Tolansky, Multiple-Beam Interferometry of Surfaces and Films (Dover Publications Inc., New York, 1970).

24. E. Spiller, J. Opt. Soc. Amer. 61, 669 (1971).

25. C.A. Parker, Photoluminescence of Solutions (Elsevier Publishing Co., New York, 1968).

26. J.B. Birks, Photophysics of Aromatic Molecules (John Wiley and Sons Ltd., New York, 1970).

27. N.S. Bayliss, J. Chem. Phys. 18, 292 (1950).

28. W. West and A.L. Geddes, J. Physical Chem. 68, 837 (1964).

29. R. Pappalardo, H. Samelson, and A. Lempicki, Appl. Phys. Letters 16, 267 (1970).

30. J.B. Marling, D.W. Gregg, and L. Wood, Appl. Phys. Letters 17, 527 (1970).

31. J. Frenkel, Kinetic Theory of Liquids (Dover Publications, Inc., New York, 1955).

32. G. Porter and M.W. Windsor, Disc. Faraday Soc. 17, 178 (1954).

33. C. Kittel, Introduction to Solid State Physics (John Wiley and Sons, Inc., New York, 1967).

34. G.L. McAllister, Dissertation, University of Southern California, 1969 (unpublished).

35. G.L. McAllister, M.M. Mann, and L.G. DeShazer, IEEE J. Quantum Elect. QE-6, 44 (1970).

36. See K. Venkataraman, The Chemistry of Synthetic Dyes (Academic Press, Inc., New York, 1952) for a classification of organic dyes.

37. Handbook of Chemistry and Physics (Chemical Rubber Publishing Co., Cleveland, Ohio, 1951).

38. M. Abramowitz and I.A. Stegun, Handbook of Mathematical Functions (Dover Publications, Inc., New York, 1965).